Quantum Radar: An Engineering Perspective

Murat Can KARAKOÇ, 1 Özgün ERSOY, 2 Ahmad SALMANOGHLI KHIAVI, 2 and Asaf Behzat ŞAHİN 2

¹⁾Department of Electrical and Electronics Engineering, Erzurum Technical University, Erzurum, Türkiye

²⁾Department of Electrical and Electronics Engineering, Ankara Yıldırım Beyazıt University, Ankara, Türkiye

(*Electronic mail: murat.karakoc@erzurum.edu.tr)

(Dated: 14 October 2025)

Quantum radar has emerged as a promising paradigm that utilizes entanglement and quantum correlations to overcome the limitations of classical detection in noisy and lossy environments. By exploiting microwave entanglement generated from superconducting devices such as Josephson parametric amplifiers, converters, and traveling-wave parametric amplifiers, quantum radar systems can achieve enhanced detection sensitivity, lower error probabilities, and greater robustness against thermal noise and jamming. This review provides a comprehensive overview of the field, beginning with the theoretical foundations of quantum illumination and extending to the generation of entanglement in the microwave regime. We then examine key quantum radar subsystems, including quantum transducers, amplification chains, and receiver architectures, which form the backbone of practical designs. Recent experimental systems are surveyed in the microwave domain, highlighting proof-of-principle demonstrations and their transition from conceptual frameworks to laboratory realizations. Collectively, the progress reviewed here demonstrates that quantum radar is evolving from a theoretical construct to a practical quantum technology capable of extending the performance boundaries of classical radar.

I. INTRODUCTION

Quantum radar systems propose to exceed the standard classical limit in terms of sensitivity and resolution through the utilization of quantum resources such as entanglement and squeezing¹. This advantage is especially relevant for detecting weakly reflecting targets under strong thermal or electronic noise, where classical systems struggle.

The primary difference lies in the nature of the transmitted and received signals. Classical radar transmits coherent microwave pulses and detects echoes through direct energy return and correlation with the transmitted waveform². Quantum radar, on the other hand, uses entangled photon pairs, where the signal is transmitted toward the target and the idler is stored ^{1,3,4}. Detection is not based on the direct return of the signal but on correlations between the returned signal and the retained idler, enabling discrimination of the target even under severe noise or loss conditions⁵.

In optical domain implementations of quantum radar, entangled photon pairs are typically generated through spontaneous parametric down-conversion (SPDC) or four-wave mixing (FWM). The signal photon is directed toward a target, while the idler (or herald) photon is retained for correlation analysis. Notable demonstrations include standoff target detection using correlated photon pairs with timing-coincidence measurements, even under strong environmental noise^{6–10}.

Various methods have been proposed to quantify the entanglement of quantum states in radar systems. Commonly used approaches include the symplectic eigenvalue test¹¹, the Peres – Horodecki – Simon criterion¹², and measures of quantum discord^{13,14}, each providing information on how quantum correlations behave under noise and loss.

The concept of microwave quantum illumination¹⁵ is based on foundational studies in reversible optical-to-microwave quantum interfaces¹⁶ and strong coupling in circuit cavity

electromechanics¹⁷, yet it remains a theoretical proposal without experimental realization. Nevertheless, it represents a paradigm shift in quantum radar, transitioning the operational domain from optics to the microwave regime, where classical radar systems operate but quantum advantages had not been practically demonstrated. Subsequent proposals introduced optoelectronic converters as an alternative route to maintain entanglement at higher temperatures and reduce reliance on mechanical interfaces¹⁸. Some experimental demonstrations using Josephson parametric devices, such as Josephson parametric amplifier (JPA), Josephson parametric converter (JPC), and Josephson traveling-wave parametric amplifier (JTWPA), have transformed quantum illumination from a theoretical proposal into a viable microwave sensing strategy^{19–21}.

The atmospheric and channel effects critically influence the performance of quantum radar. Although microwave frequencies experience less attenuation and scattering than optical frequencies, thermal noise, absorption, and turbulence can still degrade entanglement and weaken correlations^{22–24}. These processes are often modeled with cascaded beam splitters, showing how thermally excited photons reduce fidelity and shorten the entanglement lifetimes^{25,26}. Despite these challenges, recent work shows that entanglement-based sensing protocols can retain advantages over classical systems under realistic noise and loss conditions^{7,27}.

Since ideal joint measurements remain technologically challenging, experimental systems rely on hybrid receivers in which signal and idler are downconverted, digitized, and processed using high-speed analog-to-digital converters (ADCs) and FPGA-based platforms^{20,28}. This digital architecture enables real-time quadrature extraction, second-order moment analysis, and flexible post-processing strategies that approximate the performance of optimal quantum receivers.

In the following sections of this paper are organized as follows. In Sect. II, we summarize the fundamental princi-

ples of quantum illumination and its distinction from classical detection. We then discuss entanglement generation in the microwave regime, focusing on Josephson-based devices and other techniques for producing correlated microwave photons. Sect. III highlights critical building blocks such as quantum transducers, parametric amplifiers, atmospheric effects, path loss and receiver architectures. Next, in Sect. IV surveys existing implementations and proof-of-principle demonstrations, illustrating how theoretical concepts are implemented in practice. Finally, the paper concludes with a in Sect. V that outlines the current challenges, potential applications, and future directions, followed by an abbreviation list and references.

II. THEORETICAL BACKGROUNDS

A. Quantum Correlation and Non-Classicality As An Essential Key in Quantum Radar

Classical radar detects objects by comparing the amplitude and phase of reflected electromagnetic waves against a reference signal. The performance of such systems is ultimately constrained by classical noise statistics. Quantum radar, in contrast, attempts to take advantage of non-classical correlations, particularly quantum entanglement, to obtain lower error-probability in target detection, even when entanglement is largely destroyed during propagation. Entanglement turns a pair of photons into a single, delocalized information carrier, so that information acquired by measuring the return signal can be interpreted only in the light of the locally stored idler. This global description underpins protocols such as quantum illumination (QI), which theoretically achieves a signalto-noise (SNR) advantage over any classical scheme that irradiates the same mean number of photons^{1,15}. Entanglement was introduced in the 1935 Einstein-Podolsky-Rosen (EPR) paper as a challenge to the completeness of quantum mechanics²⁹. Schrödinger coined the term "entanglement" to describe states that cannot be expressed as a product of local states for individual subsystems³⁰. A pure bipartite state $|\Psi\rangle$ is entangled when its Schmidt number exceeds one³¹. For mixed states, separability is defined by the criterion $\rho = \Sigma_i p_i \rho_{Ai} \otimes \rho_{Bi}$; any state that cannot be decomposed in this form is entangled. Bell's 1964 theorem confirmed that the measurement statistics of the entangled states can violate the inequalities obeyed by all local-realist theories, thereby revealing intrinsically non-classical correlations³². In the radar context, these correlations are exploited not for provable non-locality but for enhanced hypothesis testing in noisy channels. In the following sections, various versatile criteria used to quantify quantum correlations will be discussed and analyzed in detail.

1. Selected Criteria for Quantum Correlation in Quantum Radar Systems

It should be noted that through the literature survey, it is found that there are a lot of versatile methods and approaches to study non-classicality or quantum correlation in a quantum system; some bold utilized criteria are the symplectic eigenvalue $(2\eta)^{18,33}$, Peres-Horodesky-Simon^{12,33,34}, and quantum discord^{20,35,36}; however, the reader may find other reported criteria as well. Next, we briefly discuss these criteria and attempt to apply some of them to the quantum system used in quantum radar applications.

a. Peres-Horodecki-Simon Criterion (λ_S): The Peres-Horodecki-Simon criterion is a foundational separability test used in the study of quantum entanglement, especially in CV systems¹². It originates from the Peres criterion³⁷, which states that a necessary condition for separability is that the partial transpose of the density matrix of the system remains positive (positive partial transpose, PPT). While originally framed for finite-dimensional systems, Simon extended this concept to Gaussian states using covariance matrices¹². In this context, the criterion involves applying partial transposition to the covariance matrix and checking $\lambda_S > 1$ for entanglement. This criterion is the necessary and sufficient condition for separability of the bipartite Gaussian states. Thus, it should be assumed that all the states of the cavity are Gaussian. The Peres-Horodecki-Simon test is both practical and computationally efficient, making it a standard tool for analyzing CV entanglement in quantum optics, cavity QED, and other Gaussian state-based quantum systems 12,33,34,37-39.

b. Quantum Discord: Quantum discord is a measure of quantum correlations in a bipartite quantum system that go beyond entanglement. It captures the difference between two classically equivalent expressions for mutual information when extended to the quantum domain 13,14,40. Although classical systems have only one definition of mutual information, quantum systems can exhibit discrepancies due to measurement-induced disturbance. Discord quantifies the minimum loss of correlations after a local measurement in a subsystem. A nonzero discord implies the presence of non-classical correlations, even in separable (nonentangled) states, making it a more general indicator of quantumness than entanglement alone.

Although both quantum discord and entanglement measure non-classical correlations, they differ fundamentally. Entanglement is a strict subset of quantum correlations and requires inseparability of the quantum state. Quantum discord, however, can be nonzero even in separable (unentangled) mixed states. This means that systems that are not entangled may still exhibit quantum behavior via discord. Entanglement is typically destroyed by decoherence, whereas discord is more robust in noisy environments. Thus, discord encompasses a broader class of quantum correlations, particularly useful when entanglement is too fragile or absent. In practical terms, discord can exist in situations where entanglement-based strategies fail^{13,14,40}. For comparison, one can consider Fig. 1. Although entanglement enables high-precision sensing and non-classical signal advantages, it is often fragile un-

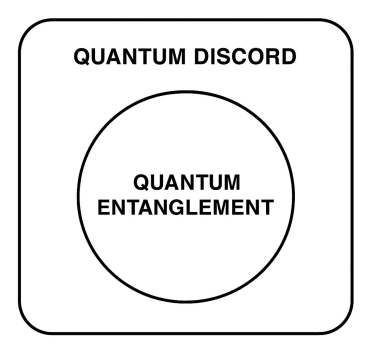


FIG. 1: Diagram representing the relationship between quantum entanglement and quantum discord. All entangled states lie within the set of discordant states, but discord can exist without entanglement.

der loss and noise, common in realistic radar channels. Quantum discord, being more resilient, offers a compelling alternative. Even when entanglement is lost, the discord may persist and contribute to enhanced target detection or reduced error probabilities. Therefore, discord-based protocols are potentially more robust for practical quantum radar applications. They provide a way to exploit quantum advantages without relying solely on entanglement, making them suitable for noisy open-system scenarios typical of radar operations ^{15,20}.

The calculation of quantum discord begins using two generalizations of classical mutual information 13,14,40,41 . Mutual information is used primarily to evaluate the total correlations between the subsystems. In the first generalization, the quantum mutual information for two systems, A and B, is defined as $I(\rho_{AB}) = S(\rho_A) + S(\rho_B) - S(\rho_{AB})$, where $S(\rho_A) = -Tr(\rho_A log_2 \rho_A)$ is the von Neumann entropy of system A, and $I(\rho_{AB})$ is the conditional von Neumann entropy 13,14,40,41 . In the following, for the system studied in this work, the first oscillator is called in a short way A, and the second is called B. Conditional entropy arises because the measurement process disturbs the state in which a physical system is set. In other words, the measurement applied to the subsystem B can change the state of the subsystem A.

The second generalization introduces the entropic quantity C(A|B), by which the classical correlation is calculated in the joint state ρ_{AB} . The classical correlation defines the maximum information about one subsystem depending on the measurement types applied to the other subsystem. The entropic quantity, considering the generalization, is defined as $C(\rho_{AB}) = S(\rho_A) - S_{min}(\rho_{AB})$, where the only difference between mutual quantum information is $S_{min}(\rho_{AB})$. That is generally described as positive operator-valued measures $(POVMs)^{13,14,40,41}$. Thus, quantum discord is usually defined as $D(\rho_{AB}) = I(\rho_{AB}) - C(\rho_{AB})$, and substituting from the above definitions it becomes $D(\rho_{AB}) = S(\rho_B) - S(\rho_{AB}) + S_{min}(A|B)$.

B. Entanglement Generation in the Microwave Regime

1. Electro-Opto-Mechanical Converter : Simon-Peres-Horodecki Criterion

In this section, we reviewed various methods that have been employed in quantum radar systems to generate entangled microwave photons, and explored different approaches to analyze the resulting non-classicality. Since generating entanglement directly in the microwave regime is experimentally challenging, one promising method is to first generate optical entanglement and then convert part of the entangled state into the microwave domain. This necessitates a hybrid quantum interface capable of mediating entanglement between optical and microwave photons. In this direction, we focus on an electro-opto-mechanical (EOM) converter^{42–44}, a system that couples optical and microwave cavities via a common mechanical resonator. In the EOM system, the mechanical element—typically a vibrational mode of a nanomembrane or drumhead-acts as a quantum bus, enabling coherent transfer of energy and quantum correlations between the optical and microwave domains. This allows us to capture both the coherent interactions and the noise dynamics critical for evaluating the entanglement transfer efficiency. Such a system plays a crucial role in future quantum networks and sensing platforms, where coherent microwave-optical interfaces are essential. The performance of EOM converters can be quantified by metrics such as cooperativity, entanglement generation rate, and transfer fidelity.

To analyze the dynamics of the system, we employ the quantum electrodynamics (QED) framework as outlined in the foundational studies^{45,46}. The analysis begins by formulating the equations of motion for the EOM converter, which constitutes a key subsystem of a typical quantum radar architecture, schematically depicted in Fig. 2. Following standard QED methodology, the Lagrangian formalism is used to systematically describe the system's behavior. The converter in Fig. 2 comprises three core components: the optical cavity (OC), the mechanical resonator (MR), and the microwave cavity (MC), all of which are dynamically coupled. To rigorously capture the full dynamics, we must first construct individual Lagrangians for each of these subsystems and then account for the interaction Lagrangians that describe their mutual couplings. This step is critical because it allows us to derive the full quantum-mechanical description of the system, including entanglement and energy exchange processes. Accordingly, the total Lagrangian of the EOM system is composed as follows:

$$\begin{split} L_{OC} &= \frac{\varepsilon_0}{2} \left(\dot{A}^2 - \omega_c^2 A^2 \right) \\ L_{MR} &= \frac{1}{2} m \dot{X}^2 - \frac{1}{2} m \omega_m^2 X^2 \\ L_{MC} &= \frac{1}{2} C(x) \dot{\phi}^2 - \frac{1}{2L} \phi^2 + \frac{1}{2} C_d \left(v_d - \dot{\phi} \right)^2 \\ L_{OC-MR} &= -\alpha_c A \dot{X} \end{split} \tag{1}$$

In this equation, the total Lagrangian is $L_{tot} = L_{OC} + L_{MR} + L_{MC} + L_{OC-MR}$ where L_{OC} , L_{MR} , L_{MC} , and L_{OC-MR} are the op-

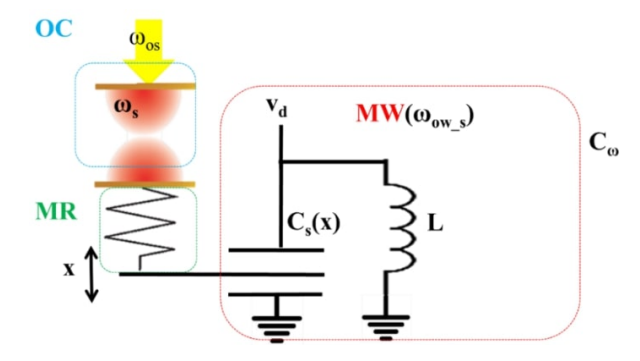


FIG. 2: EOM converter; coupling subsystems contain OC, MC, and MR⁴⁷.

tical cavity, microresonator, microcavity, and the optical cavity - the microrsonator interaction Lagrangian, respectively. In addition, the microwave cavity and the Lagrangian microresonator interaction are defined by C(x) in L_{MC} . In Eq. 1, α_C , ω_m , ω_C , L, V_d , C(x), C_d and m are the coupling coefficient between the OC and the MR, the angular frequency of the oscillation of the MR, the resonance frequency of the optical cavity, the inductance of the microwave circuit, the external driving field applied to the MC and the components of the LC circuit, namely the variable and fixed capacitors, as well as the effective mass of the mechanical resonator. Furthermore, the symbols A, X, and ϕ denote the vector potential, the mechanical resonator position operator, and the magnetic flux operator, respectively, each of which plays a critical role in the quantum dynamics of the system. In the subsequent step, the Hamiltonian formalism must be developed to fully describe the energy dynamics of the system. This involves identifying the conjugate momentum operators corresponding to the canonical variables A, X, and ϕ , based on the classical definition of conjugate variables⁴⁸. Once the canonical pairs are established, the creation (\hat{a}^{\dagger}) and annihilation (\hat{a}) operators are introduced to quantize the fields. These operators enable a compact and tractable representation of the system's quantum Hamiltonian, which is then rewritten in the operator formalism as:

$$\begin{split} H_{OC} &= \hbar \omega_c \hat{a}_c^{\dagger} \hat{a}_c \\ H_{MR} &= \frac{\hbar \omega_m}{2} \left(\hat{p}_x^2 + \hat{q}_x^2 \right) \\ H_{MC} &= \hbar \omega_\omega \hat{c}_\omega^{\dagger} \hat{c}_\omega - j V_d C_d \sqrt{\frac{\hbar \omega_\omega}{2C_t}} \left(\hat{c}_\omega - \hat{c}_\omega^{\dagger} \right) \\ H_{OC-MR} &= \hbar \sqrt{\frac{\alpha_c^2 \omega_m}{2\epsilon_0 \omega_c m}} \left(\hat{a}_c^{\dagger} + \hat{a}_c \right) \hat{p}_x \\ H_{MC-MR} &= C_p C_t \frac{\hbar \omega_\omega}{2} \sqrt{\frac{\hbar}{\omega_m m}} \hat{q}_x \left(\hat{c}_s - \hat{c}_s^{\dagger} \right)^2 \\ H_{OC-\text{drive}} &= i\hbar E_c \left(\hat{a}_c^{\dagger} e^{(-j\omega_L t)} - \hat{a}_c e^{(j\omega_L t)} \right) \end{split} \tag{2}$$

In Eq. 2, $(\hat{a}_c^{\dagger}, \hat{a}_c)$ and $(\hat{c}_{\omega}^{\dagger}, \hat{c}_{\omega})$ the optical and microwave cavities contribute to the creation and annihilation operators, respectively. In addition, E_c and \hbar are the input driving rate of the optical cavity and the reduced Planck constant, respectively. Moreover, C_p and C_t are derived using

 $C_p = C'(x)/[C(x) + C_d]^2$ and $C_t = C_d + C(x_0)$, where x_0 denotes the equilibrium position of the MR. In Eq. 2, the second term within the microwave cavity Hamiltonian H_{MC} represents the influence of an externally applied driving field on the cavity. Importantly, this expression explicitly includes the interaction Hamiltonians that describe the coupling between the OC and the MR, as well as between the MC and the MR. These terms are critical because they reveal how the coupling between subsystems is mediated via the mechanical resonator. By adjusting the relevant parameters, such as coupling strengths, detuning frequencies, or drive powers, one can dynamically control the interaction strengths between the cavities. This, in turn, provides a direct mechanism for modulating the degree of entanglement between the optical and microwave modes, a key requirement for efficient quantum transduction and hybrid quantum network applications. The equations of motion for this system can be systematically derived using the Heisenberg-Langevin formalism^{47,49}, which incorporates both unitary evolution and open system dynamics. An essential aspect of this approach is accounting for the interaction between the system and its environment, which introduces dissipation and quantum noise. These are modeled using input noise operators and damping terms, allowing for a realistic description of decoherence. Once the environmental effects are properly included, the complete set of quantum Langevin equations can be written as:

$$\begin{split} \dot{a}_{s} &= -\left(j\Delta_{c} + \kappa_{c}\right)\hat{a}_{c} - jG_{1}\hat{p}_{x} + E_{c} + \sqrt{2\kappa_{s}}\hat{a}_{in} \\ \dot{c}_{\omega} &= -\left(j\Delta_{\omega} + \kappa_{\omega}\right)\hat{c}_{\omega} + j\Delta_{o\omega 1}G_{2}\hat{q}_{x}\hat{c}_{\omega} + E_{\omega} + \sqrt{2\kappa_{cs}}\hat{c}_{in} \\ \dot{q}_{x} &= \omega_{m}\hat{p}_{x} + G_{1}\left(\hat{a}_{c} + \hat{a}_{c}\right) \\ \dot{p}_{x} &= -\gamma_{m}\hat{p}_{x} - \omega_{m}\hat{q}_{x} + \Delta_{\omega}G_{2}\hat{c}_{\omega}^{\dagger}\hat{c}_{\omega} + \hat{b}_{in} \end{split}$$

$$(3)$$

In this equation, κ_c , γ_m , κ_w , Δ_c , and Δ_ω are the damping rate of OC, MR and MC and the related de-tuning frequencies, respectively. Also, $G_1 = \sqrt{\alpha_c^2 \omega_m / 2\varepsilon_0 m \omega_c}$, $G_2 = C_p C_t \sqrt{\hbar/s}$, and $E_{\omega} = V_d C_d \sqrt{w_w/2\hbar C_t}$. The optical cavity driving field is given as $E_c = \sqrt{2P_c \kappa_c \hbar \omega_L}$, where P_c represents the excitation power applied to drive the cavities ^{18,50}. Eq. 3 is a non-linear operator equation, which generally cannot be solved analytically in terms of the full quantum operators of the system due to its complex interaction terWs and quantum noise contributions. In order to proceed, a common and effective technique is to linearize the dynamics around a steady-state operating point. This is achieved by assuming the system is driven by a strong coherent field, which allows one to decompose each operator into its classical steady-state mean (DC component) and small quantum fluctuations around that mean. Such an approximation is valid when the driving field is sufficiently strong, causing the quantum field dynamics to remain close to the classical operating point. This method, often referred to as linearization around the fixed point, is widely used in cavity optomechanics and quantum transduction analyzes 18,51. Consequently, each cavity mode operator (for both optical and microwave fields) can be rewritten as $a_c = A_s + \delta a_c$, $c_w = C_s + \delta c_\omega$, $q_x = X_s + \delta q_x$, and $P_x = p_x + \delta p_x$, where capitalized variables with the subscript "s" denote the steadystate (DC) solutions of the system, i.e., the operating point values when the cavities are driven by a continuous external field. Delta-prefix operators, such as $\delta a(t)$, represent the quantum fluctuations around these fixed-point solutions. By substituting these linearized expressions into the nonlinear equation (3), and retaining only the first-order terms in the fluctuation operators (i.e., neglecting higher-order nonlinear fluctuation terms), one obtains a linearized set of equations that describe the dynamics of the system near the steady state. This approach isolates the stationary regime behavior, allowing analytical treatment of quantum noise, stability, entanglement generation, and signal transduction characteristics. The resulting linearized equations—commonly referred to as the quantum Langevin equations in fluctuation form — are foundational for studying quantum correlations and noise spectra in driven - dissipative hybrid systems. These expressions form the basis for calculating key performance metrics such as squeezing levels, entanglement rates, and transduction efficiency. Then Eq. 3 is expressed as:

$$-(j\Delta_{c} + \kappa_{c})A_{s} - jG_{1}P_{s} + E_{c} = 0$$

$$-(j\Delta_{\omega} + \kappa_{\omega})C_{s} + j\Delta_{o\omega 1}G_{2}X_{s}C_{s} + E_{\omega} = 0$$

$$\omega_{m}P_{s} + 2G_{1}\operatorname{Re}\left\{A_{s}\right\} = 0$$

$$-\gamma_{m}P_{s} - \omega_{m}X_{s} + \Delta_{\omega}G_{2}\left|C_{s}\right|^{2} = 0$$
(4)

In order to solve Eq. 4, it is typically assumed that $\{A_s\} \gg 1$ and $|C_s| \gg 1$. The steady-state values of the system variables $-A_s$, C_s , P_s , and X_s - are then determined accordingly:

$$P_{s} = \frac{2G_{1}\operatorname{Re}\{A_{s}\}}{\omega_{m}}, X_{s} = \frac{-\gamma_{m}P_{s} + \Delta_{\omega}G_{2}|C_{s}|^{2}}{\omega_{m}}$$

$$A_{s} = \frac{E_{c} - jG_{1}P_{s}}{(j\Delta_{c} + \kappa_{c})}, C_{s} = \frac{j\Delta_{\omega\omega_{1}}G_{2}X_{s}C_{s} + E_{\omega}}{(j\Delta_{\omega} + \kappa_{\omega})}$$
(5)

Equation 5 specifies the steady-state conditions, also known as DC operating points, at which the cavities are subject to external driving. Our analysis that follows is primarily concerned with examining small perturbations occurring around these equilibrium states. It can be demonstrated without difficulty that the selection of DC operating points in Equation 5 does not affect the behavior of these perturbations. Therefore, the differential equations describing the dynamics of the mode perturbations in proximity to these steady-state values, represented by $(A_s, P_s, X_s, \text{and } C_s)$, are formulated as follows:

$$\delta \dot{a}_{s} = -\left(j\Delta_{c} + \kappa_{c}\right) \hat{\delta}a_{c} - iG_{1}\hat{\delta}p_{x} + \sqrt{2\kappa_{s}}\hat{\delta}a_{in}
\delta \dot{c}_{\omega} = i\Delta_{\omega 1}G_{2} \left\{ \hat{\delta}q_{x}C_{s} + X_{s}\hat{\delta}c_{\omega} \right\} + \sqrt{2\kappa_{cs}}\hat{\delta}c_{in} - \left(i\Delta_{\omega} + \kappa_{\omega}\right) \hat{\delta}c_{\omega}
\delta \dot{q}_{x} = \omega_{m}\hat{\delta}p_{x} + G_{1} \left(\hat{\delta}a_{c} + \hat{\delta}a_{c}\right)
\delta \dot{p}_{x} = -\gamma_{m}\hat{\delta}p_{x} + \Delta_{\omega}G_{2} \left\{ \hat{\delta}c_{\omega}^{+}C_{s} + C_{s}^{*}\hat{\delta}c_{\omega} \right\} - \omega_{m}\hat{\delta}q_{x} + \hat{\delta}b_{in}$$
(6)

In Eq. 6 represents the linearized set of coupled equations that describe the quantum fluctuations of the cavity modes. By solving these equations, one can analyze both the separability and the degree of entanglement among the modes. The interaction between the cavity modes in the converter facilitates the generation of CV entanglement, which manifests itself as quantum correlations between the quadrature operators of the intra-cavity fields^{23,52,53}. This entanglement is fundamentally governed by the coupling coefficients, which can be engineered to tailor the correlation strength and structure among the cavity modes. In particular, Eq. 6 shows that the fluctuation δp_x couples to δa_c through the coupling constant G_1 , δw_c is influenced by δq_x through the term $C_sG_2\Delta w_1$, δq_x driven

by changes in δX_c , and finally δp_x is modulated by both δq_x and δw_c . It is therefore the responsibility of the quantum radar system designer to appropriately select and tune these coupling parameters to establish the desired quantum correlations between modes. The influence of these parameters on the degree of mode entanglement will be thoroughly investigated in the following section. Note that in Eq. 6, the OC and MC modes are represented solely using annihilation operators, whereas for the MR, the quadrature operators are used. This distinction enables the straightforward derivation of the quadrature representations for the OC and MC modes. Accordingly, the full system dynamics can be compactly expressed using the QED formalism in matrix form:

$$\begin{bmatrix} \delta \dot{q}_{x} \\ \delta \dot{p}_{x} \\ \delta \dot{X}_{c} \\ \delta \dot{Y}_{c} \\ \delta \dot{Y}_{\omega} \end{bmatrix} = \underbrace{\begin{bmatrix} 0 & \omega_{m} & G_{1}\sqrt{2} & 0 & 0 & 0 & 0 \\ -\omega_{m} & -\gamma_{m} & 0 & G_{m} & 0 & 0 & 0 \\ 0 & 0 & -\kappa_{c} & \Delta_{c} & 0 & 0 & 0 \\ 0 & -G_{1}\sqrt{2} & -\Delta_{c} & -\kappa_{c} & 0 & 0 & 0 \\ G_{11} & 0 & 0 & 0 & -\kappa_{\omega 1} & \Delta_{\omega 1} \\ G_{22} & 0 & 0 & 0 & -\Delta_{\omega 1} & -\kappa_{\omega 1} \end{bmatrix}}_{A_{i,i}} \times \underbrace{\begin{bmatrix} \delta q_{x} \\ \delta p_{x} \\ \delta X_{c} \\ \delta Y_{c} \\ \delta X_{w} \\ \delta Y_{w} \end{bmatrix}}_{\mathbf{u}(0)} + \underbrace{\begin{bmatrix} 0 \\ \delta b_{in} \\ \sqrt{2\kappa_{c}} \delta X_{c}^{in} \\ \sqrt{2\kappa_{c}} \delta Y_{c}^{in} \\ \sqrt{2\kappa_{\omega}} \delta Y_{w}^{in} \end{bmatrix}}_{\mathbf{n}(t)}$$

$$(7)$$

The parameters used in this equation are defined as $G_m = \sqrt{2G_2\Delta_{\omega}C_s}$, $G_{11} = -\sqrt{2G_2\Delta_{\omega}\operatorname{Im}\{C_s\}}$, $G_{22} = \sqrt{2G_2\Delta_{\omega}\operatorname{Re}\{C_s\}}$, $\kappa_{\omega 1} = \kappa_{\omega} + G_2\Delta_{\omega}\operatorname{Im}\{q_s\}$, and $\Delta_{\omega 1} = \kappa_{\omega} + G_2\Delta_{\omega}\operatorname{Im}\{q_s\}$

 $\Delta_{\omega} - G_2 \Delta_{\omega} \operatorname{Re} \{q_s\}$. One can consider the solution of Eq. 7, which is $u(t) = e^{(A_{i,j}t)}u(0) + \int e^{(A_{i,j}s)}n(t-s)ds$, where n(.) defines the noise of the system. The familiar correlation function can be applied to characterize the noises in the system as 18,46,49,52 :

$$\langle a_{in}(s)a_{in}^{*}(s') \rangle = [N(\omega_{c}) + 1] \delta(s - s'); \langle a_{in}^{*}(s)a_{in}(s') \rangle = [N(\omega_{c})] \delta(s - s')$$

$$\langle c_{in}(s)c_{in}^{*}(s') \rangle = [N(\omega_{\omega}) + 1] \delta(s - s'); \langle c_{in}^{*}(s)c_{in}(s') \rangle = [N(\omega_{\omega})] \delta(s - s')$$

$$\langle b_{in}(s)b_{in}^{*}(s') \rangle = [N(\omega_{m}) + 1] \delta(s - s'); \langle b_{in}^{*}(s)b_{in}(s') \rangle = [N(\omega_{m})] \delta(s - s')$$

$$(8)$$

In Eq. 8, $\left[e^{(\hbar w/k_BT)}-1\right]^{-1}$, where T and k_B denote the operational temperature and the Boltzmann constant, respectively. This function $N(\omega)$ represents the mean number of thermal photons in thermal equilibrium for a mode of frequency ω . In Eq. 7 describes the fluctuations of the cavity modes and forms the basis for analyzing mode entanglement. In the context of quantum radar applications, special emphasis is placed on the entanglement between the OC and MC modes, as it plays a critical role in the overall performance

and sensitivity of the system. Accordingly, our focus is directed toward quantifying and characterizing the correlation between the OC and MC modes. To achieve this, all potential factors that may degrade or destroy the entanglement between modes are thoroughly examined. The degree of entanglement is assessed using the Simon-Peres-Horodecki criterion, which provides a necessary and sufficient condition for CV bipartite entanglement^{12,33,37,38}:

$$\lambda_{SPH} = \det(A) \cdot \det(B) + (0.25 - |\det(C)|)^2 - \operatorname{tr}(AJCJBJC^TJ) - 0.25 \times (\det(A) + \det(B)) \ge 0$$
(9)

In Eq. 9, J is a matrix like J = [0,1;-1,0], and "tr" represents the matrix trace operation. The criterion presented in Eq. 9 serves as a necessary and sufficient condition for the separability of bipartite Gaussian states. Consequently, the analysis assumes that all the cavity states considered exhibit

Gaussian statistics. In Eq. 10, the matrices A, B and C represent the local covariance matrices and the cross-correlation matrix, respectively, forming the full covariance matrix in the block structure $J = [A, C; C^T, B]$. The elements of the mentioned matrix are exemplified for the OC-MC modes as:

$$A = \begin{bmatrix} \langle \delta X_c^2 \rangle - \langle \delta X_c \rangle^2 & 0.5 \times \langle \delta X_c \delta Y_c + \delta Y_c \delta X_c \rangle - \langle \delta X_c \rangle \langle \delta Y_c \rangle \\ 0.5 \times \langle \delta X_c \delta Y_c + \delta Y_c \delta X_c \rangle - \langle \delta X_c \rangle \delta Y_c \rangle & \langle \delta Y_c^2 \rangle - \langle \delta Y_c \rangle 2 \end{bmatrix}$$

$$B = \begin{bmatrix} \langle \delta X_\omega^2 \rangle - \langle \delta X_\omega \rangle^2 & 0.5 \times \langle \delta X_\omega \delta Y_\omega + \delta Y_\omega \delta X_\omega \rangle - \langle \delta X_\omega \rangle \langle \delta Y_\omega \rangle \\ 0.5 \times \langle \delta Y_\omega \delta X_\omega + \delta X_\omega \delta Y_\omega \rangle - \langle \delta Y_\omega \rangle \langle \delta X_\omega \rangle & \langle \delta Y_\omega^2 \rangle - \langle \delta Y_\omega \rangle \rangle \end{bmatrix}$$

$$C = \begin{bmatrix} 0.5 \times \langle \delta X_c \delta X_\omega + \delta X_\omega \delta X_c \rangle - \langle \delta X_c \rangle \langle \delta X_\omega \rangle & 0.5 \times \langle \delta X_c \delta Y_\omega + \delta Y_\omega \delta X_c \rangle - \langle \delta X_c \rangle \delta Y_\omega \rangle \\ 0.5 \times \langle \delta Y_c \delta X_\omega + \delta X_\omega \delta Y_c \rangle - \langle \delta Y_c \rangle \delta X_\omega \rangle & 0.5 \times \langle \delta Y_c \delta Y_\omega + \delta Y_\omega \delta Y_c \rangle - \langle \delta Y_c \rangle \langle \delta Y_\omega \rangle \end{bmatrix}$$

$$(10)$$

For each two-mode entanglement evaluation, we need to

construct matrix elements and use criterion expressed in Eq.

9 to analyze the correlation between modes. For doing so, the calculation of the quadrature modes operators expectation value $(\langle \delta X_c \rangle, \langle \delta X_\omega \rangle, \langle \delta X_c^2 \rangle, \langle \delta X_\omega^2 \rangle)$ are necessary to study the modes entanglement.

The influence of key parameters in the tripartite system, namely MR damping rate, incident wavelength, and temperature, on the entanglement between cavity modes is systematically investigated. The impact of temperature on the system is presented in Fig. 3a. As expected, increasing the system's temperature leads to a significant reduction in entanglement, ultimately causing the cavity modes to become separable. Detailed behavior at 200 mK and 300 mK is highlighted in the magnified inset.

A critical factor limiting the operation of the tripartite system to cryogenic temperatures is the relatively low resonance frequency of the MR cavity ($w_m = 2\pi \times 10^6$). According to Eq. 8 thermal noise becomes dominant at such low frequencies, severely degrading entanglement. To address this issue, several approaches have been proposed, including frequency band engineering and replacing the MR with a high-frequency optoelectronic component⁴⁷. Therefore, to maintain entanglement, the operational temperature should remain below approximately 1200 mK. Another crucial parameter affecting entanglement is the wavelength of the excitation source. As shown in Fig. 3b, varying the incident wavelength modulates the degree of entanglement between the cavity modes. In Fig. 3c, the effect of the MR damping rate on the cavity modes of the OC and MC is analyzed, revealing that the entanglement is highly sensitive to this rate. This sensitivity arises from the role of the MR oscillator in mediating the coupling between the optical and microwave cavities. For further insight, Fig. 3d shows the entanglement between the MR and OC modes as a function of the MR damping rate. As the damping increases, the coupling between MR and OC weakens, leading to a pronounced deterioration in the entanglement.

Thus far, the dynamics of the EOM converter have been analytically derived using the canonical quantization method in conjunction with the Heisenberg-Langevin formalism. However, in a practical quantum radar scenario, the system must be able to transmit entangled microwave photons toward a remote target. This implies that the entangled photons will propagate through the atmosphere before interacting with the target. Naturally, similar to classical radar systems, signal dispersion and degradation occur during atmospheric propagation. To counteract this loss, an amplifier may be used to boost the signal strength prior to atmospheric transmission. However, amplifying entangled photons while preserving their quantum correlations presents a significant challenge. Quantum amplification must avoid introducing excessive noise that could degrade the non-classical correlations. Furthermore, after interacting with the target, the scattered photons once again traverse the atmospheric channel, may be amplified, and are ultimately detected. In the next stage of this work, another quantum device that can be used to generate non-classicality will be discussed in detail using quantum theory, along with the other criterion to analyze the quantum entanglement generated.

2. Opto-Electronic Converter System Definition: Symplectic Eigenvalue Criterion (2η)

The proposed optoelectronic system, depicted in Fig. 4, comprises an optical cavity, a photodetector, a varactor diode (VD), and an inductor¹⁸. In this configuration, the OC mode is initially coupled to the photodetector, which generates a photocurrent dependent on the incident photon energy represented as $i = f_1(\hbar \omega)$, where f_1 denotes the optical coupling function. The resulting photocurrent is then directed through a varactor diode, leading to a change in its capacitance, described by $C = f_2(\hbar \omega)$, with f_2 acting as the electrical coupling factor. This capacitance variation directly influences the resonance frequency of the MC, effectively linking it to the optical input. Thus, the system enables a direct and tunable interaction between the optical and microwave cavity modes via optoelectronic mediation. The photodetector's responsivity characteristics are illustrated in Fig. 4b, while Fig. 4c presents a representative model of the varactor diode, showing how its capacitance varies with the applied voltage. These two figures serve to demonstrate typical device responses and are not tied to a specific implementation. Fig. 4d further clarifies the dynamic interaction chain: the optical cavity couples to the photodetector, which influences the varactor diode through the photocurrent, thus modulating the parameters of the MC. Here, A_{ω} represent the amplitude and frequency of the MC mode, respectively, while ω_c and A_c denote the frequency and amplitude of the OC mode. Crucially, the degree of coupling between the two cavity modes is governed by the tuning of the coupling functions f_1 and f_2 . The ratio f_1/f_2 quantifies the extent of the influence of the OC mode on the MC mode. By appropriately engineering this ratio, the system can establish and sustain entanglement between the cavity modes, even under room-temperature conditions, marking a significant advancement in practical quantum information processing and optoelectronic integration. From a system engineering perspective, the converter's ability to sustain and manipulate nonclassical correlations, such as CV entanglement, relies on careful optimization of both coupling paths. In the theoretical analysis that follows, the expressions for these coupling factors are derived and their impact on the entanglement between output modes is examined. In summary, the opto-electronic converter operates as an entanglement interface between the optical and microwave domains. By tuning the opto-electronic and electromagnetic coupling parameters, the degree and nature of the quantum correlations between the OC and MC modes can be precisely engineered to suit the needs of a quantum radar system¹⁸. In the following section, a theoretical design of the optoelectronic converter is presented, following a methodology similar to that used in the design of the EOM converter previously discussed. The primary objective is to perform a comprehensive comparison between the two systems with the aim of determining which architecture more effectively maintains entanglement between modes. In addition, strategies are developed to improve non-classical correlations within each system¹⁸. Given that a central focus of this research is the realization of sustainable entanglement, it is essential to develop a system architecture that not only facilitates quantum corre-

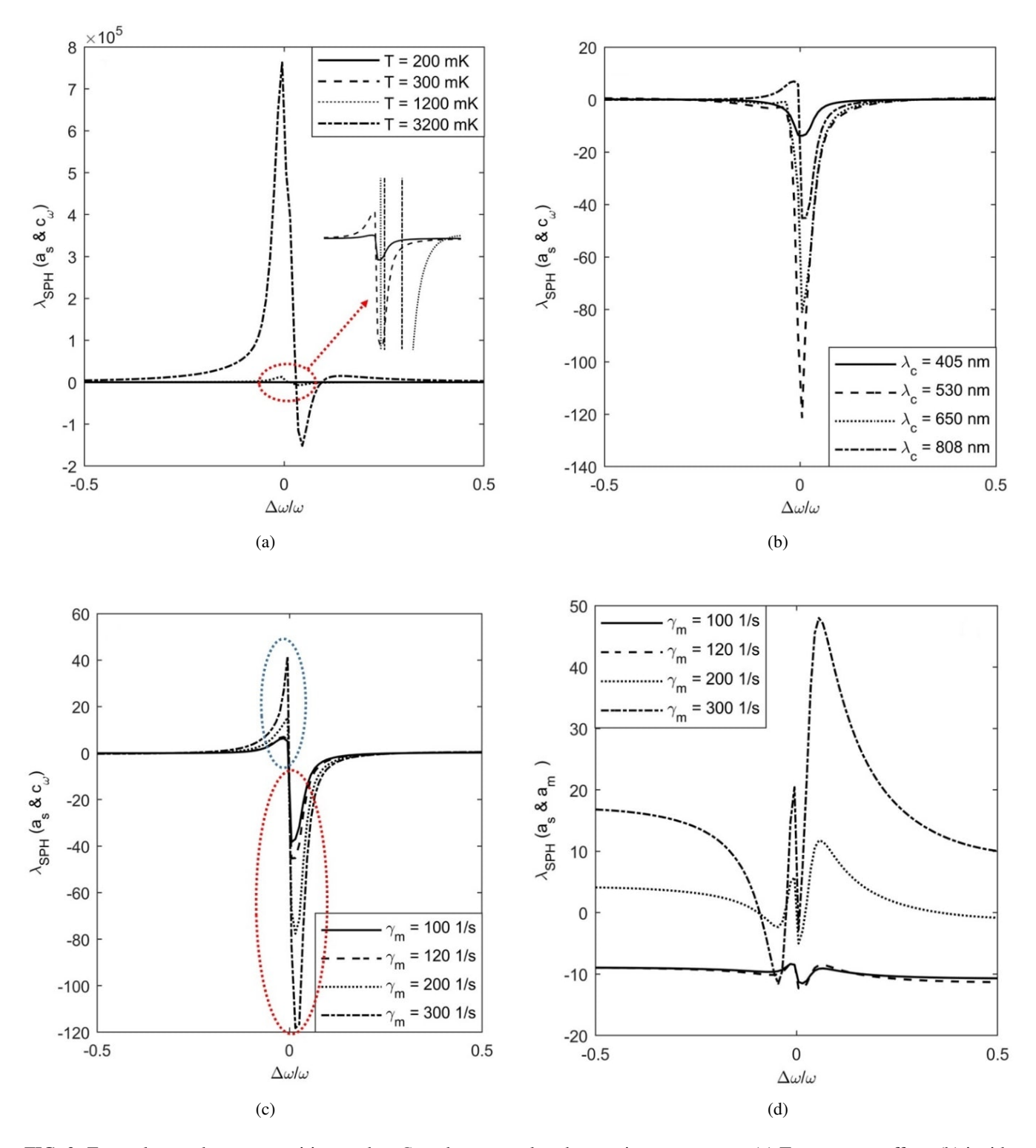


FIG. 3: Entanglement between cavities modes; C_s and q_s are real under varying parameters: (a) Temperature effect, (b) incident source wavelength effect, (c), and (d) study of the effect of the MR⁴⁷.

lations but also preserves them under practical operating conditions. This comparative study will provide critical insight into the advantages and limitations of each type of converter, guiding the optimal design of quantum interfaces for radar and

sensing applications. The quantum system incorporating the opto-electronic converter, as illustrated in Fig. 4a, is theoretically analyzed using the canonical quantization method¹⁸. Unlike the dipole approximation approach^{26,54}, which typi-

cally simplifies the interaction between light and matter, the canonical quantization framework emphasizes the full quantum interaction between the incident field and the atomic (or matter-based) system. In general, accurately describing the dynamics of any quantum system requires specifying the total Hamiltonian governing its evolution. Accordingly, the total Hamiltonian for the proposed system is formulated as follows:

$$H_{OC} = \frac{e_0}{2} \left(E^2 + \omega_c^2 A^2 \right)$$

$$H_{PD} = \frac{P^2}{2m_{eff}} + \frac{1}{2} m_{eff} \omega_{eg}^2 X^2$$

$$H_{MC} = \frac{Q^2}{2C_0} + \frac{\phi^2}{2L} + \frac{C_d v_d}{C_0} Q$$

$$H_{OC-PD} = \alpha_c \frac{AP}{m_{eff}}$$

$$H_{MC-PD} = \frac{-C'(x)}{C_0^2} \left\{ \frac{Q^2}{2} + C_d v_d Q \right\} X$$
(11)

In Eq. 11, the operators (X, P), (A, E), and (ϕ, Q) represent the position and momentum of the electron-hole pairs in the photodetector (PD), the vector potential and electric field of the optical cavity, and the phase and charge operators associated with the MC, respectively. These constants α_c , ω_{eg} , v_d , and C'(x), C_0 , C_d , and m_{eff} correspond to the optical-to-microwave cavity coupling coefficient, the PD gaprelated transition frequency, the driving voltage of the MC, the position-dependent variable capacitance, the total capacitance, the capacitance between the MC and its driving field, and the effective mass of the electron-hole pair, respectively. To proceed, it is necessary to identify the canonical conjugate variables for A, X, and ϕ to express the Hamiltonian of the system in terms of the creation and annihilation operators. This step follows the classical approach of defining conjugate pairs as outlined in⁴⁶. The resulting Hamiltonian, reformulated using these quantized variables, is then given by:

$$H_{OC} = \hbar \omega_{c} \hat{a}_{c}^{\dagger} \hat{a}_{c} + j\hbar E_{c} \left[\hat{a}_{c}^{\dagger} e^{(-j\omega_{oc}t)} - \hat{a}_{c} e^{(j\omega_{oc}t)} \right]$$

$$H_{MR} = \frac{\hbar \omega_{eg}}{2} \left(\hat{p}_{x}^{2} + \hat{q}_{x}^{2} \right)$$

$$H_{MC} = \hbar \omega_{\omega} \hat{c}_{\omega}^{\dagger} \hat{c}_{\omega} - j |v_{d}| C_{d} \sqrt{\frac{\hbar \omega_{\omega}}{2C_{0}}} \left[\hat{c}_{\omega} e^{(-j\omega_{o\omega}t)} - \hat{c}_{\omega}^{\dagger} e^{(j\omega_{o\omega}t)} \right]$$

$$H_{OC-PD} = \hbar \sqrt{\frac{\alpha_{c}^{2} \omega_{eg}}{2\varepsilon_{0} m_{eff} \omega_{c}}} \left(\hat{a}_{c}^{\dagger} + \hat{a}_{c} \right) \hat{p}_{x}$$

$$H_{MC-PD} = -\frac{\hbar \mu_{c} \omega_{\omega}}{2d} \sqrt{\frac{\hbar}{\omega_{eg} m_{eff}}} \hat{q}_{x} \hat{c}_{s}^{\dagger} \hat{c}_{s}$$

$$(12)$$

In Eq. 12, (a_c^{\dagger}, a_c) , and $(c_{\omega}^{\dagger}, c_{\omega})$ denote the creation and annihilation operators for the optical and microwave cavity modes, respectively. These parameters ω_{oc} , (p_x, q_x) , E_c , g_{op} , and d represent the angular frequency of the input optical source, the normalized quadrature operators, the drive amplitude of the input optical cavity, the optical coupling rate between the cavity and the photodetector, and the width of the VD capacitor depletion layer, respectively. Moreover, $\mu_c = C'(x)/C_0$ captures the sensitivity of the variable capacitance to electron-hole displacement. In the Hamiltonian HMC-PD interaction, which describes the coupling between the microwave cavity and the photodetector, the key coupling strength is given by $g_{\alpha,\rho} = (\mu_c \omega_\omega/2 d) \times \sqrt{(\hbar/\omega_{eg} m_{eff})}$. This coupling factor, g_{ow} , plays a crucial role in the quantum radar architecture, as it allows for strong manipulation of nonclassical correlations between modes. Notably, by tuning this parameter, it becomes possible to maintain entanglement between the optical and microwave modes even under elevated thermal noise conditions, a point that will be further examined in the Results and Discussion section. The optical coupling rate between the OC and the PD is given similarly by $g_{op} = \sqrt{(\omega_{\rm eg} \alpha_{\rm c}^2/2\omega_{\rm c}\varepsilon_0 \, {\rm m_{eff}})}$. In Eq. 12, the Hamiltonian HMC incorporates both the free evolution of the microwave cavity field and its external drive. One of the key analytical tasks in this framework is the accurate determination of the coupling coefficient between the optical cavity and the photodetector. To this end, within a unit volume, first-order perturbation theory can be used, and the resulting expression is provided as follows⁵⁷:

$$g_{op} = \frac{\pi \omega_{t}}{\varepsilon_{0} V_{m}} \mu^{2} g_{J} \left(\hbar \omega_{eg} \right) \cdot L \left(\omega_{eg} \right) \rightarrow \alpha_{c} = \sqrt{\frac{2 \omega_{c} \varepsilon_{0} \, m_{eff}}{\omega_{eg}} \frac{\pi \omega_{c}}{\varepsilon_{0} V_{m}} \mu^{2} g_{J} \left(\hbar \omega_{eg} \right) \cdot L \left(\omega_{eg} \right)}$$
(13)

In this expression, $g_J(\hbar\omega_{eg})$, μ , and $L(\omega_{eg})$ represent the density of the states of the photodetector, the dipole moment, and the Lorentzian line-shaped function, respectively. Eq. 12 also provides information on the behavior of the coupling constant α_c , which is highly sensitive to the electrical and optical properties of the photodetector. Therefore, engineering the converter, particularly the design and material composition of

the PD, offers an effective means of modulating the strength of the coupling between the OC and the PD. As an example, plasmonic-based photodetectors can be employed to significantly enhance the optical coupling factor due to their strong light-matter interaction at the nanoscale⁵⁷. Ultimately, this coupling constant serves as a critical design parameter for engineering the interaction between cavity modes and control-

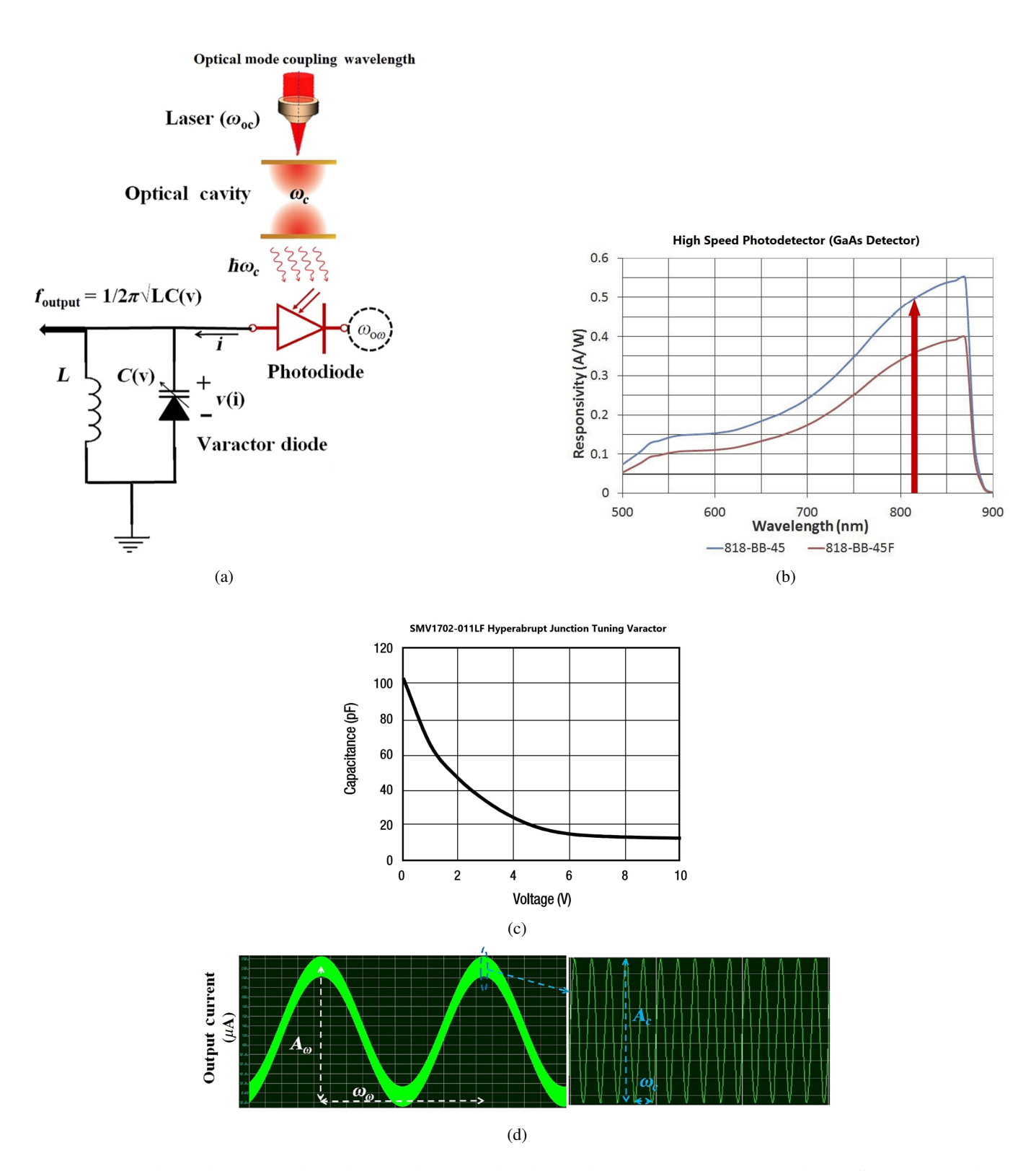


FIG. 4: Optoelectronic system schematic; C_s and q_s are real under varying parameters: (a) OC mode coupling to MC mode through the photodetector and a Varactor diode, (b) a typical GaAs photodetector responsivity graph⁵⁵, (c) Varactor diode capacitance variation vs biased voltage, which is the function of photodetector current⁵⁶ and (d) simulated photocurrent as a function of optical cavity mode incidence wave frequency and amplitude. The optical mode center wavelength is around 808 nm^{18} .

ling the degree of non-classical correlations, such as entanglement, in the quantum radar system. Following the derivation of the system Hamiltonian, the corresponding equations of motion are formulated using the Heisenberg-Langevin formalism. To accurately capture the real behavior of the system, damping rates and noise terms are incorporated to account for dissipation and fluctuations arising from the interaction between the quantum system and its surrounding environment. Furthermore, applying the rotating wave approximation (RWA), we define the relevant detuning parameters as follows: the detuning between the microwave cavity and its drive is $\Delta_{\omega} = \omega_{\omega} - \omega_{o\omega}$, the optical cavity detuning is $\Delta_c = \omega_c - \omega_{oc}$, and the photodetector detuning is $\Delta_{eg} = \omega_{eg} - \omega_c$. With these considerations, the complete set of dynamical equations for the newly proposed opto-electronic converter is established as:

$$\begin{aligned}
\dot{a_c} &= -\left(j\Delta_c + \kappa_c\right)\hat{a_c} - jg_{op}\hat{p_x}\hat{a_c} + E_c + \sqrt{2\kappa_c}\hat{a_{in}} \\
\dot{c_\omega} &= -\left(j\Delta_\omega + \kappa_\omega\right)\hat{c_\omega} + jg_{\omega p}\hat{a_x}\hat{c_\omega} + E_\omega + \sqrt{2\kappa_\omega}\hat{c_{in}} \\
\dot{q_x} &= \Delta_{eg}\hat{p_x} + g_{op}\left(\hat{a_c^\dagger} + \hat{a_c}\right) \\
\dot{p_x} &= -\gamma_p\hat{p_x} - \Delta_{eg}\hat{q_x} + g_{\omega p}\hat{c_\omega^\dagger}\hat{c_\omega} + \hat{b}_{in}
\end{aligned} \tag{14}$$

In Eq. 14, the parameters κ_c , γ_p , and κ_ω are the damping rates of the optical cavity, photodetector, and microwave cavity, respectively. Furthermore, Δ_c , Δ_ω , and Δ_{eg} are the related detuning frequencies, and $v_d C_d \sqrt{(\omega_\omega/2\hbar C_0)}$

and $E_c = \sqrt{(2P_c \kappa_c/\hbar\omega_{oc})}$, where P_c is the OC excitation power^{18,48,50,51}. In addition, b_{in} is the quantum noise attributed to PD acting on it and ain and c_{in} are input noises due to the fact that cavities interact with the environment. In the following analysis, we focus on evaluating the entanglement between the OC and MC as continuous-mode quantum fluctuations around their fixed operating points, where both cavities are externally driven. Under these steady state conditions, the system's equations of motion can be linearized by expanding around the classical (steady state) fields, which serve as fixed points^{18,51}. To carry out this linearization, each cavity mode is expressed as a sum of a steady-state component and a small fluctuation term, as follows: $a_c = A_s + \delta_{ac}$, $c_{\omega} = C_s + \delta c \omega$, $q_x = X_s + \delta q_x$, and $p_x = P_s + \delta p_x$. In these equations, capital letters with the subscript 's' denote the steady-state (fixedpoint) values, while the δ terms represent small quantum fluctuations around those operating points. For the purpose of evaluating non-classical correlations, such as entanglement, only the fluctuation components need to be considered, as they capture the essential quantum behavior of the system. Nevertheless, it is necessary first to derive the linearized equations of motion under steady-state conditions. This linearization typically assumes certain conditions to ensure system stability, such as Re $\{A_s\} \gg 1$ and $|C_s| \gg 1$. In the following analysis, we focus exclusively on the quantum fluctuations and solve the corresponding linearized equations. The quantum fluctuations of the cavity modes are thus analyzed in the vicinity of their respective steady-state values $(A_s, P_s, X_s, \text{ and } C_s)$ as:

$$\delta \dot{a}_{s} = -\left(j\Delta_{c} + \kappa_{c}\right)\delta\hat{a}_{c} - jg_{op}\left\{A_{s}\delta\hat{p}_{x} + \hat{p}_{s}\delta\hat{a}_{c}\right\} + \sqrt{2\kappa_{c}}\delta\hat{a}_{in}$$

$$\delta \dot{c}_{\omega} = -\left(j\Delta_{\omega} + \kappa_{\omega}\right)\delta\hat{c}_{\omega} + jg_{\omega p}\left\{\delta\hat{q}_{x}C_{s} + X_{s}\delta\hat{c}_{\omega}\right\} + \sqrt{2\kappa_{cs}}\delta\hat{c}_{in}$$

$$\delta \dot{q}_{x} = \Delta_{eg}\delta\hat{p}_{x} + g_{op}\left\{\delta\hat{a}_{c}^{\dagger} + \delta\hat{a}_{c}\right\}$$

$$\delta \dot{p}_{x} = -\gamma_{p}\delta\hat{p}_{x} - \Delta_{eg}\delta\hat{q}_{x} + g_{\omega p}\left\{C_{s}\delta\hat{c}_{\omega}^{\dagger} + C_{s}^{*}\delta\hat{c}_{\omega}\right\} + \delta\hat{b}_{in}$$
(15)

The CV entanglement can arise from the interaction between cavity modes^{18,48,50,51}. In order to analyze the entanglement specifically between the OC and MC, it is essential to

define the corresponding quadrature fluctuations, which serve as the primary modes of interest. The matrix representation of these quadrature operators is given by:

$$\begin{bmatrix} \dot{\delta q_x} \\ \dot{\delta p_x} \\ \dot{\delta X_c} \\ \dot{\delta Y_c} \\ \dot{\delta Y_w} \end{bmatrix} = \underbrace{\begin{bmatrix} 0 & \Delta_{eg} & \sqrt{2}g_{op} & 0 & 0 & 0 \\ -\Delta_{eg} & -\gamma_p & 0 & 0 & \sqrt{2}g_{\omega p}C_{sr} & -\sqrt{2}g_{\omega p}C_{si} \\ 0 & \sqrt{2}g_{op}A_{si} & -\kappa_c & \Delta_c + g_{op}P_s & 0 & 0 \\ 0 & -\sqrt{2}g_{op}A_{sr} & -\Delta_c - g_{op}P_s & -\kappa_c & 0 & 0 \\ 0 & -\sqrt{2}g_{\omega p}C_{si} & 0 & 0 & 0 & -\kappa_{\omega} & \Delta_{\omega} - g_{wp}q_s \\ -\sqrt{2}g_{wp}C_{sr} & 0 & 0 & 0 & -\Delta_{\omega} - g_{wp}q_s & -\kappa_{\omega} \end{bmatrix}}_{A_{ij}} \underbrace{\begin{bmatrix} \delta q_x \\ \delta p_x \\ \delta X_c \\ \delta Y_c \\ \delta X_w \\ \delta Y_w \end{bmatrix}}_{u(0)} + \underbrace{\begin{bmatrix} 0 \\ \delta b_{in} \\ \sqrt{2}\kappa_c \delta X_c^{in} \\ \sqrt{2}\kappa_c \delta Y_c^{in} \\ \sqrt{2}\kappa_\omega \delta Y_w^{in} \\ \sqrt{2}\kappa_\omega \delta Y_w^{in} \end{bmatrix}}_{n(t)}$$

$$(16)$$

In Eq. 16, δX_c^{in} , δY_c^{in} , δX_ω^{in} , and δY_ω^{in} are the noise quadra-

ture operator. The solution of Eq. 16 produces an equa-

tion with a form as " $u(t) = e^{(A_{i,j})}u(0) + \int (e^{(A_{i,j}s)}n(t-s))ds$ ", where n(s) is the noise. For this equation, the input noises

obey the correlation function^{18,48,50,51}. The entanglement between the cavity modes can be quantitatively analyzed using the Symplectic eigenvalue criterion, as described in^{12,58}:

$$\eta = \frac{1}{\sqrt{2}} \sqrt{\sigma \pm \sqrt{\sigma^2 - 2\det(\sigma)}}, \sigma = \det(A) + \det(B) - 2\det(C)$$
(17)

Eq. 17 justifies that " $2\eta >= 1$ " stands for separability of modes; otherwise, two modes become entangled ¹².

Two-mode entanglement between the mode a_c and c_{ω} as well as between a_c and c_b is analyzed under the conditions of $\mu_c = 0.0002$ and a transmitter-detector distance $D_{td} = 20$ m. In this context (see Fig. 4a, a_c represents the OC mode, c_w denotes the MC mode, and c_h corresponds to the backscattered mode of the target prior to detection. The results are illustrated in Fig. 5, where the entanglement measure 2η is plotted as a function of the PD detuning frequency. A peak in entanglement is observed near $\Delta_{eg} \approx 0$, indicating that the PD is optimally excited when its frequency ω_c is nearly resonant with the transition frequency ω_{eg} . As shown in Fig. 5a, significant entanglement persists even when the cavity temperature T_c reaches 3500 mK. This finding challenges a well-known limitation of traditional tripartite systems, which are typically used for generating entangled photons: at elevated temperatures, thermally excited photons degrade entanglement. However, once the MC-generated photons propagate through the atmosphere toward the target, the signal becomes unpredictable due to environmental effects and targetinduced scattering. These influences are modeled using Eq. 17, with the results shown in Fig. 5b. It becomes evident that for $T_c > 1000mK$, the returned backscattered signals become completely separable, and entanglement vanishes. Therefore, particular attention must be given to the subsystem responsible for generating entangled photons. Although the effects of atmospheric propagation and target scattering cannot be controlled, a carefully designed subsystem can mitigate their impact⁵⁹. By enabling entangled-state generation at elevated temperatures, such a design helps counteract the detrimental effects of environmental noise and preserve the quantum correlations essential for detection and communication tasks.

Another important factor here is the sensitivity of the variable capacitance to the electron-hole displacement labeled with μ_c . It is clearly evident in Fig. 6 that increasing the coupling strength between MC and PD leads to a substantial enhancement in the entanglement between the quantum states. This coupling plays a pivotal role in distinguishing the present approach, which relies on conventional tripartite systems where such coupling was either minimal or not actively optimized. To better highlight this behavior, a zoomed-in view of the critical region is provided in the inset of the Fig. 6. The enhanced MC–PD coupling not only strengthens quantum correlations but also facilitates the preservation of entangled states at elevated operational temperatures. This capability marks a significant step toward practical quantum sensing

and communication in real-world environments. Specifically, the stronger coupling helps to overcome the detrimental effects of thermal noise that typically degrade entanglement in conventional setups. This makes the system⁵⁹ highly suitable for applications in quantum radar, secure communication, and remote sensing, where environmental control is limited and maintaining quantum coherence is critical.

The nonclassicality generated (squeezing effect) due to the quantum system presented is another important effect that one needs to consider. Fig. 7 illustrates the variation of the entanglement measure 2η as a function of the detuning frequency Δ_{eg} , at an operational temperature of 500 mK. Two distinct entanglement regimes are highlighted. Near $\Delta_{eg} = -2.05 \times 105$ Hz, a sharp peak in 2η is observed, indicating a strong entangled state when PD is nearly resonant with the atomic transition frequency ω_{eg} . This strong entanglement is attributed to optimal coupling between the MC and PD modes, enabling coherent quantum correlations. The corresponding quadrature distribution (marked in yellow) shows a well-elongated elliptical shape along the X_{ω} axis, suggesting strong phase-sensitive correlations. In contrast, at $\Delta_{eg} = -7.2 \times 107$ Hz, the system exhibits a much weaker entanglement, with $2\eta \approx 1$, which signifies nearly separable states. The corresponding quadrature distribution (marked in blue) appears more circular and localized, indicating reduced squeezing and weaker correlations. These results confirm that optimal detuning is critical to maximize the degree of entanglement and highlight the system's sensitivity to coupling-induced frequency alignment. This tunability could be exploited in practical implementations to maintain entanglement under varying operational or environmental conditions.

Up to this point, the dynamics of the quantum radar system incorporating the opto-electronic converter have been analytically derived using the canonical quantization method and Heisenberg-Langevin equations. The Symplectic eigenvalue criterion has been applied as a robust tool for evaluating the entanglement between cavity modes. Following the entanglement analysis of the converter modes outlined according to the system architecture in Figs. 5, 6 and 7. A central objective of this system was to demonstrate that the converter shown in Fig. 4a can be designed such that these environmental effects do not completely destroy the entanglement between modes. One notable distinction between the opto-electronic and electro-opto-mechanical converters lies in the treatment of signal amplification. As highlighted in Fig. 4a, this system deliberately omits any amplifier or active medium. This design choice is based on findings from the lit-

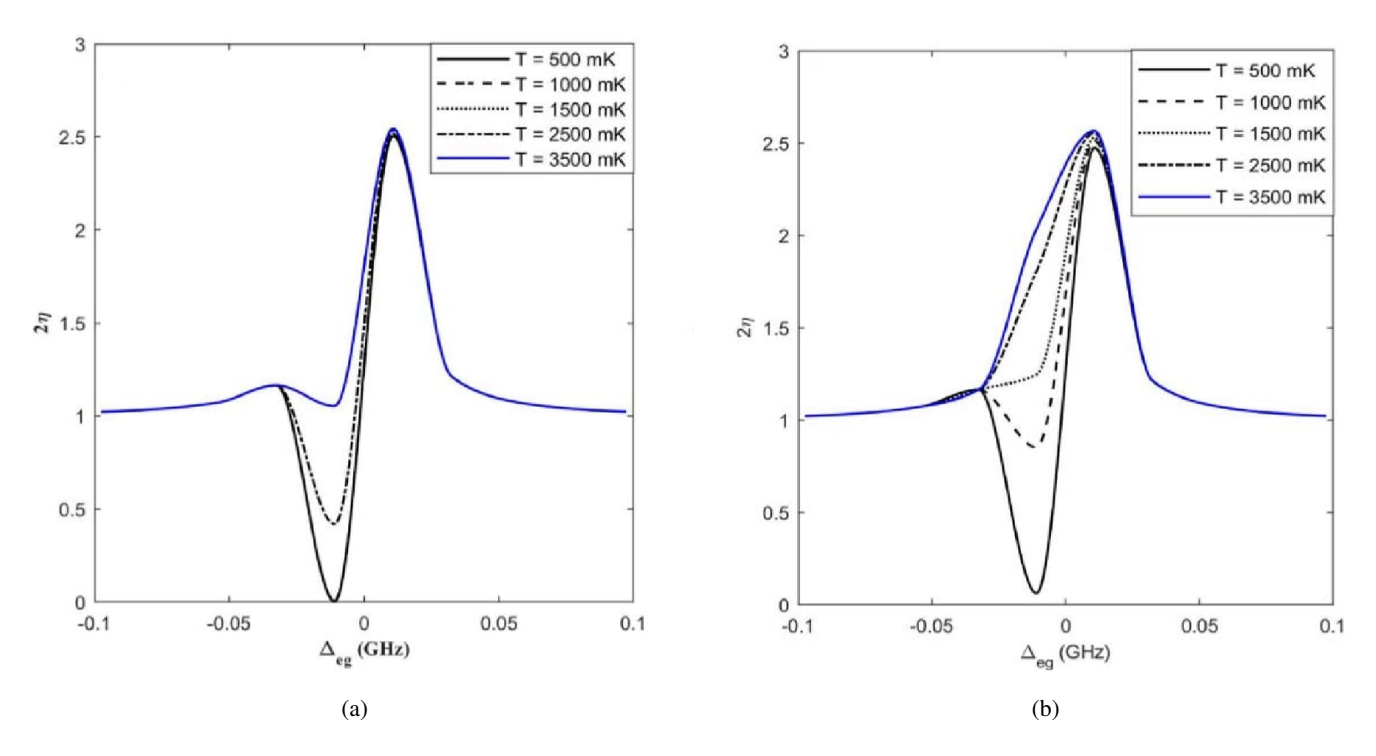


FIG. 5: Temperature effect on entanglement between: (a) a_c and c_{ω} , (b) a_c and c_b for $\mu_c = 0.0002$ and $D_{td} = 20$ m $\kappa_{atm} = 2 \times 10^{-6}$ 1/m, and $\kappa_t = 18.2$ 1/m⁵⁹.

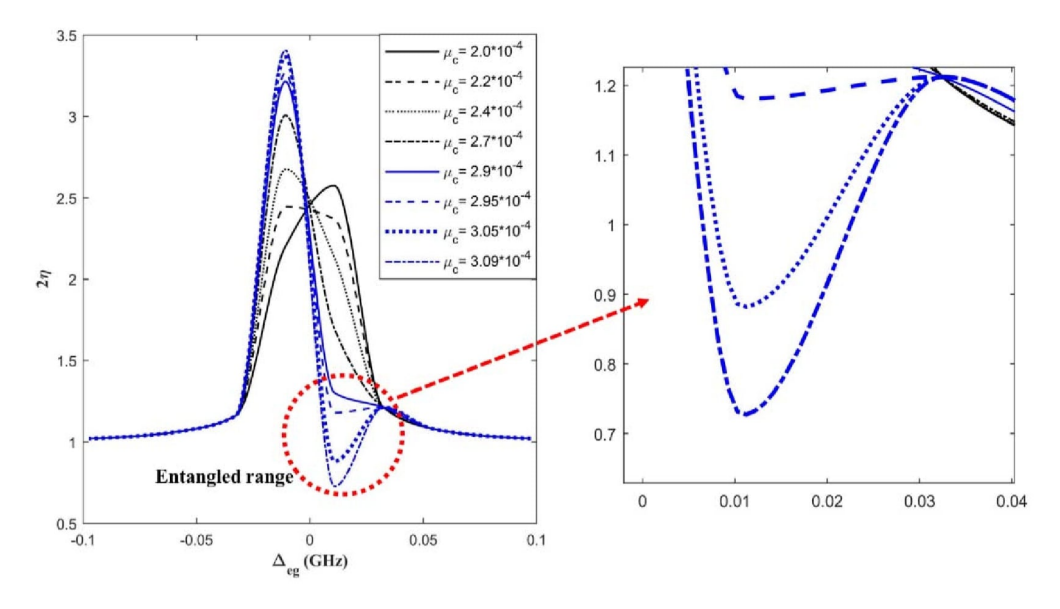


FIG. 6: MC-PD coupling effect on entanglement between a_c and c_{ω} at $T_c = 5000mK$ and $D_{td} = 20 \text{ m}^{59}$.

erature, which indicate that amplifying entangled microwave photons—particularly to increase photon number while preserving quantum correlations—is extremely challenging and often introduces additional noise that can severely degrade entanglement³⁴. Therefore, the focus of opto-electronic system was to show that a quantum radar system based on this converter can function effectively without requiring amplification, and more importantly, that it can preserve the entangle-

ment of the photons during atmospheric propagation and prior to detecting the backscattered signal. This highlights a critical advantage of this system architecture in terms of preserving quantum correlations in realistic operational scenarios.

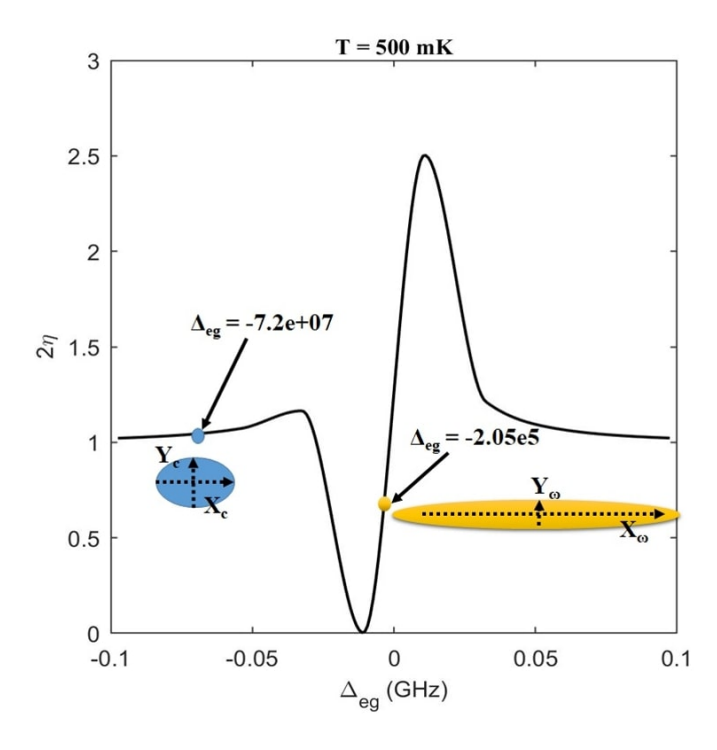


FIG. 7: Entanglement measure 2η versus detuning frequency Δ_{eg} at a fixed temperature of 500 mK. A pronounced peak in entanglement is observed near $\Delta_{eg} = -2.05 \times 105$ Hz, corresponding to strong quantum correlations between cavity modes. Inset ellipses show quadrature phase-space representations at selected detuning points: the yellow ellipse (right) indicates highly squeezed, entangled states, while the blue ellipse (left) represents weaker entanglement with reduced squeezing. These findings emphasize the critical role of detuning in tuning and preserving entanglement.

3. Design of A Single Josephson Junction JPA to Create Entangled Photons: Quantum Discord

A single JJ can function as a parametric amplifier by leveraging its intrinsic nonlinearity to enable energy transfer between electromagnetic modes. Fundamentally, a JJ consists of two superconducting electrodes separated by a thin insulating barrier, allowing Cooper pairs to tunnel through via the Josephson effect^{60–67}. The junction exhibits non-linear inductance, which is the key ingredient for parametric amplification. When driven by an external pump tone at frequency f_{pump} , the non-linear inductance modulates periodically, allowing for energy exchange between different frequency components. This parametric process can lead to degenerate or non-degenerate amplification 60–67. In degenerate mode, the signal and idler share the same frequency but have a phase relationship that governs the gain. In non-degenerate mode, the idler frequency is different from the signal, leading to greater operational flexibility. This process is governed by the quantum Langevin equation and the input-output formalism, where the interaction Hamiltonian describes the coupling between the pump, signal, and idler fields. The strength of amplification is dictated by the critical current, I_c , of the junction, its shunt capacitance, and the external impedance environment⁶⁸. These parameters influence the bandwidth, gain, and stability of the amplifier. The gain mechanism is fundamentally based on parametric conversion, where the pump injects energy into

the signal and idler fields while maintaining overall energy conservation. In the following, this review article centers on the theoretical analysis of single-JJ and arrayed-JJ JPAs, as well as emerging JPA architectures, and compares simulation and modeling results with existing findings in the literature.

Firstly, a single JJ JPA is quantum-mechanically analyzed and it attempts to theoretically derive amplifier critical parameters such as gain. The approach begins with the theoretical derivation of the system's Hamiltonian, followed by an analysis of the dynamics using the quantum Langevin equation. The Hamiltonian of the lumped element JPA (that is, a capacitively shunted JJ coupled to a transmission line 69) is expressed as (setting $\hbar=1$ for the reminder of the article):

$$H_{\rm JPA} = \frac{\hat{\mathcal{Q}}^2}{2C} - E_J \cos(\hat{\phi}) \longrightarrow \approx \omega_0 \hat{a}^{\dagger} \hat{a} + \frac{\Lambda}{6} \left(\hat{a}^{\dagger} + \hat{a} \right)^4 \quad (18)$$

where C, E_J , Q, and ϕ are the capacitance, Josephson energy, charge, and phase across the junction, respectively. The other side of the arrow is obtained by expanding the cosine to the fourth order and introducing annihilation and creation operators $(\hat{a}, \hat{a}^{\dagger})$. In this equation, the Kerr coefficient $\Lambda = -\frac{E_c}{2}$ and the bare frequency of the resonator $\omega = \sqrt{8E_cE_J}$, where $E_c = \frac{e^2}{2C}$ is the charging energy of the Josephson junction. Using these definitions, the Hamiltonian of a single Josephson junction JPA driven by a monochromatic current pump^{68,70} is expressed as:

$$H_{CP} = H_{JPA} + \varepsilon e^{(-jw_p t)} \hat{a}^{\dagger} + \varepsilon^* e^{(jw_p t)} \hat{a}$$
 (19)

where ε and ω_p are the amplitude of the drive pump and its frequency, respectively. To simplify successive algebra, it becomes versatile to eliminate the pump Hamiltonian using a displacement operator such as $a=\alpha+\delta a$, where α and δa are the classic field and quantum fluctuation, respectively. In the displaced frame mentioned above, the Hamiltonian of the system becomes:

$$H_{CP} = \Delta_0 \, \delta \hat{a}^{\dagger} \delta \hat{a} + \frac{\lambda_1}{2} \, \delta \hat{a}^{\dagger 2} + \frac{\lambda_1^*}{2} \, \delta \hat{a}^2 + H_{nc} \qquad (20)$$

In Eq. 20 the shifted detuning is $\Delta_0 = \omega_0 + 4|\alpha|^2 \Lambda - \omega_p$, and the effective parametric pump strength is $\lambda_1 = 2\alpha^2 \Lambda$, and also the classical field can be solved using the quantum Langevin equation⁶⁹. Finally, the last term in the equation, H_{nc} , is the nonlinear correction Hamiltonian arising from the displacement of the Kerr nonlinearity and can be written as:

$$H_{nc} = \mu_0 \,\delta \hat{a}^{\dagger 2} \delta \hat{a} + \mu_0^* \,\delta \hat{a}^{\dagger} \delta \hat{a}^2 + \Lambda \,\delta \hat{a}^{\dagger 2} \delta \hat{a}^2 \qquad (21)$$

where $\mu_0 = 2\alpha^2\Lambda$ is the cubic term coefficient. However, to obtain a linear equation, one can ignore H_{nc} for the small quantum fluctuation, which is valid in the low-gain and low

Kerr nonlinearity regime⁶⁹. It is notable to indicate that the output state of the JPA pumped with a monochromatic current, regarding Eq. 20 and Eq. 21, is a displaced squeezed state. In the following, it is focused on Eq. 21 by ignoring H_{nc} , and using the input-output formula $(\delta \hat{a}_{\text{out}} = \sqrt{\kappa} \delta \hat{a} - \delta \hat{a}_{\text{in}})^{69}$, attempt to analytically calculate the gain of the system. Generally, the behavior of the intracavity mode may be calculated by the master equation method; still, one can use the quantum Langevin equation for a single-mode cavity as:

$$\frac{d\delta\hat{a}}{dt} = -j\left[\delta\hat{a}, (H_{CP} - H_{nc})\right] - \frac{\kappa}{2}\delta\hat{a} + \sqrt{\kappa}\delta\hat{a}_{\text{in}}$$
 (22)

where κ and $\delta \hat{a}_{\rm in}$ are the JPA damping constant created due to any mismatching between the JPA and the environment, and the embedded quantum fluctuation of the external field applied to the system, respectively. Eq. 22 can be expanded for $\delta \hat{a}$ and its conjugate as:

$$\frac{d\delta\hat{a}}{dt} = -\left(j\Delta_0 + \frac{\kappa}{2}\right)\delta\hat{a} - j\lambda_1\delta\hat{a}^\dagger + \sqrt{\kappa}\delta\hat{a}_{\rm in}$$
 (23)

$$\frac{d \,\delta \hat{a}^{\dagger}}{dt} = -\left(-j\Delta_0 + \frac{\kappa}{2}\right) \delta \hat{a}^{\dagger} + j\lambda_1^* \,\delta \hat{a} + \sqrt{\kappa} \,\delta \hat{a}_{\rm in}^{\dagger} \qquad (24)$$

In Eq. 23 and 24 are linear and, in terms of frequency components $\left(a(\omega) = \frac{1}{\sqrt{2\pi}} \int a(t)e^{j\omega t}dt\right)$, becomes:

$$-j\omega \,\delta\hat{a}(\omega) = -\left(j\Delta_0 + \frac{\kappa}{2}\right)\delta\hat{a}(\omega) - j\lambda_1\delta\hat{a}^{\dagger}(-\omega) + \sqrt{\kappa}\,\delta\hat{a}_{\rm in}(\omega) \tag{25}$$

$$j\omega \,\delta \hat{a}^{\dagger}(-\omega) = -\left(-j\Delta_0 + \frac{\kappa}{2}\right) \delta \hat{a}^{\dagger}(-\omega) + j\lambda_1^* \delta \hat{a}(\omega) + \sqrt{\kappa} \,\delta \hat{a}_{\rm in}^{\dagger}(-\omega) \tag{26}$$

The last step to calculate the gain is to establish the relating scattering matrix, then employing the input-output formula, the gain of the signal and idler can be calculated 61,71,72 . It is shown as follows:

$$\begin{cases}
\left[-j(\omega + \Delta_{0}) + \frac{\kappa}{2}\right] \delta \hat{a}(\omega) + j\lambda_{1} \delta \hat{a}^{\dagger}(-\omega) = \sqrt{\kappa} \delta \hat{a}_{\text{in}}(\omega), \\
\left[j(\omega - \Delta_{0}) + \frac{\kappa}{2}\right] \delta \hat{a}^{\dagger}(-\omega) - j\lambda_{1}^{*} \delta \hat{a}(\omega) = \sqrt{\kappa} \delta \hat{a}_{\text{in}}^{\dagger}(-\omega)
\end{cases}$$

$$\Rightarrow \begin{bmatrix} \delta \hat{a}_{\text{out}}(\omega) \\ \delta \hat{a}_{\text{out}}^{\dagger}(-\omega) \end{bmatrix} = \begin{cases} \kappa \begin{bmatrix} -j(\omega + \Delta_{0}) + \frac{\kappa}{2} & j\lambda_{1} \\ -j\lambda_{1}^{*} & j(\omega - \Delta_{0}) + \frac{\kappa}{2} \end{bmatrix}^{-1} - \begin{pmatrix} 1 & 0 \\ 0 & 1 \end{pmatrix} \end{cases} \begin{bmatrix} \delta \hat{a}_{\text{in}}(\omega) \\ \delta \hat{a}_{\text{in}}^{\dagger}(-\omega) \end{bmatrix}$$
(27)

Finally, the gain matrix is presented as:

$$\begin{bmatrix} \delta \hat{a}_{\text{out}}(\boldsymbol{\omega}) \\ \delta \hat{a}_{\text{out}}^{\dagger}(-\boldsymbol{\omega}) \end{bmatrix} = \begin{bmatrix} \frac{\kappa \left[j(\boldsymbol{\omega} - \Delta_0) + \frac{\kappa}{2} \right]}{\frac{\kappa^2}{4} - i\kappa\Delta_0 + \boldsymbol{\omega}^2 - \Delta_0^2} - 1 & \frac{-j\lambda_1 \kappa}{\frac{\kappa^2}{4} - j\kappa\Delta_0 + \boldsymbol{\omega}^2 - \Delta_0^2} \\ \frac{j\lambda_1^* \kappa}{\frac{\kappa^2}{4} - j\kappa\Delta_0 + \boldsymbol{\omega}^2 - \Delta_0^2} & \frac{\kappa \left[-i(\boldsymbol{\omega} + \Delta_0) + \frac{\kappa}{2} \right]}{\frac{\kappa^2}{4} - j\kappa\Delta_0 + \boldsymbol{\omega}^2 - \Delta_0^2} - 1 \end{bmatrix} \begin{bmatrix} \delta \hat{a}_{\text{in}}(\boldsymbol{\omega}) \\ \delta \hat{a}_{\text{in}}^{\dagger}(-\boldsymbol{\omega}) \end{bmatrix}$$
(28)

where the matrix element (1,1) determines the signal gain and the element (1,2) signifies the idler gain. It should be noted that the effective parametric pump strength affects the idler gain, not the signal gain; in contrast, the signal gain depends on the decay of the quantum system and the frequency detuning. The gain of the single JJ JPA is defined as:

$$G_{\text{single_JJ_JPA}} = \left\{ \frac{\kappa \left[j(\omega - \Delta_0) + \frac{\kappa}{2} \right]}{\frac{\kappa^2}{4} - j\kappa\Delta_0 + \omega^2 - \Delta_0^2} - 1 \right\} - \left\{ \frac{-j\lambda \kappa}{\frac{\kappa^2}{4} - j\kappa\Delta_0 + \omega^2 - \Delta_0^2} \right\}$$
(29)

where the first part signifies the signal gain and the second part determines the idler gain. Fortunately, a compact formula can be presented for two-mode squeezed thermal states (zero-mean Gaussian states) to reduce the covariance matrix (CM) into the standard form^{73–75}. Consequently, the CM of the selected modes in the system can be presented in the form of the following matrix:

$$V_{AB} = \begin{pmatrix} (\tau b + \eta)\mathbf{I} & \sqrt{\tau(b^2 - 1)}\mathbf{C} \\ \sqrt{\tau(b^2 - 1)}\mathbf{C} & b\mathbf{I} \end{pmatrix}$$
(30)

where $\mathbf{I} \equiv \mathrm{diag}(1,1)$, $\mathbf{C} \equiv \mathrm{diag}(1,-1)$, $a = n_{o1} + 0.5$, $b = n_{o2} + 0.5$, $\tau = d_{o12}^2/(b^2-1)$, $\eta = a - (b_2^* d_{o12}^2/(b^2-1))^{73-75}$. In these equations, a and b are the expectation values of the I/Q signals for two oscillators, derived as $a = \langle I_1(\omega)I_1(\omega)\rangle = \langle Q_1(\omega)Q_1(\omega)\rangle$, $b = \langle I_2(\omega)I_2(\omega)\rangle = \langle Q_2(\omega)Q_2(\omega)\rangle$, where $I = \frac{\delta \hat{a}_i^\dagger + \delta \hat{a}_i}{\sqrt{2}}$, $Q = \frac{\delta \hat{a}_i - \delta \hat{a}_i^\dagger}{j\sqrt{2}}$, i = 1, 2.

The parameters n_{o1} , n_{o2} , and d_{o12} are the output mean photon numbers of the first and second oscillator, and the cross-correlation (phase-sensitive), respectively. One can use the input-output formula⁴⁷ to calculate the output mean photon numbers, $n_{o1} = 2\kappa_1 \langle \delta a_1^{\dagger} \delta a_1 \rangle + \langle \delta a_{\text{in-1}}^{\dagger} \delta a_{\text{in-1}} \rangle$, $n_{o2} = 2\kappa_2 \langle \delta a_2^{\dagger} \delta a_2 \rangle + \langle \delta a_{\text{in-2}}^{\dagger} \delta a_{\text{in-2}} \rangle$, $d_{o12} = 2\sqrt{\kappa_1 \kappa_2} \langle \delta a_1 \delta a_2 \rangle$. Finally, the mean photon numbers of the oscillators are $n_1 \equiv \langle \delta a_1^{\dagger} \delta a_1 \rangle$, $n_2 \equiv \langle \delta a_2^{\dagger} \delta a_2 \rangle$, $d_{12} \equiv \langle \delta a_1 \delta a_2 \rangle$, where n_1 , n_2 , and d_{12} represent the first oscillator mean photon number, and the cross-correlation between the two oscillators, respectively. It is assumed that d_{12} is real-valued.

The output entropy associated with heterodyne detection is equal to the average entropy of the output ensemble A^{73-75} . Since entropy is invariant under displacements, it can be written $\operatorname{as} S(A_{\operatorname{hetero}}) = h(\tau + \eta)$, where $h(x) \equiv (x+0.5) \log_2(x+0.5) - (x-0.5) \log_2(x-0.5)$. The von Neumann entropy of an n-mode Gaussian state with CM V_{AB} is $S(V_{AB}) = \sum_{i=1}^N f(v_i)$, where v_i are the symplectic eigenvalues. However, there is a heterodyne detection for which it is optimal for minimization of the output entropy, so the Gaussian discord is opti-

mal. The "Gaussian quantum discord" of a two-mode Gaussian state ρ_{AB} , assuming a two-mode squeezed thermal state in this study, can be defined as the quantum discord satisfying the conditional entropy restricted to the generalized Gaussian POVMs on B³⁴.

Finally, the compact form of quantum discord, classical correlation, and quantum mutual information are given, respectively, by $D(\rho_{AB}) = h(b) - h(v_-) - h(v_+) + h(\tau + \eta)$, $C(\rho_{AB}) = h(a) - h(\tau + \eta)$, $I(\rho_{AB}) = h(a) - h(v_-) - h(v_+)$, where v_\pm is the Symplectic eigenvalue of the CM. The Symplectic eigenvalues are defined as $v_\pm = \frac{\Delta \pm \sqrt{\Delta^2 - 4D}}{2}$, where $\Delta = \det(a\mathbf{I}) + \det(b\mathbf{I}) + 2\det(d_{o12}\mathbf{I})$, and $D = \det(V_{AB})$; in the recent formulas $\det\{\cdot\}$ stands for the matrix determinant.

In the compact form of the equation defined for the quantum discord, the first term stands for the von Neumann entropy of the second oscillator in the system. The second and third terms define the von Neumann conditional entropy of the system. The last term in the equation is the effect of the classical correlation depending on the type of measurement performed on the second oscillator. As a result, in the system defined, the second oscillator entropy and the off-diagonal elements in the CM significantly affect the system's quantum discord. Therefore, particular attention is paid to the interference between oscillators, and an analysis is conducted to determine which quantities may affect the quantum discord. Perhaps the other critical factor that may be considered to enhance the quantum discord is $h(\tau + \eta)$, by which the classical correlation is decreased. As mentioned in $^{73-75}$, this critical factor strongly depends on the type of measurements.

The Wigner function, $W(\beta)$, visualized over the complex phase-space coordinates $\text{Re}(\beta)$ and $\text{Im}(\beta)$, illustrates how the quantum state evolves as g increases from 0.3 to 0.5 in Fig. 8. For low g, the state remains relatively isotropic, indicating limited squeezing. As g increases, the Wigner function becomes more elongated and tilted, indicating stronger phase-sensitive squeezing and the emergence of nonclassical features—hallmarks of quantum entanglement potential. Notably, at g=0.5, the state becomes highly squeezed along one axis, confirming the amplifier's ability to generate highly cor-

related photon pairs. This figure confirms that by adjusting the parametric interaction strength, the JPA can transition from a thermal-like state to a nonclassical squeezed state, a crucial feature for quantum information processing and entangled photon generation.

III. QUANTUM RADAR SUBSYSTEMS

A. Quantum Transmitter

In quantum radar systems, the quantum transducer plays a pivotal role in enabling coherent and efficient interfacing between the microwave and optical domains¹⁵. This is essential in architectures where entangled microwave signals - used to detect a target - must be stored, converted, or measured via optical systems due to their superior detection efficiency and transmission properties.

In this context, a quantum transducer is a device capable of bidirectional and phase-coherent conversion between microwave and optical photons, ideally without adding thermal noise or decoherence. The fundamental mechanism underpinning this conversion is the tripartite interaction among microwave, mechanical, and optical modes, a framework known as electro-optomechanics or opto-electro-mechanics.

In a typical implementation, the EOM transducer consists of a mechanical resonator that simultaneously couples to both a superconducting microwave cavity and an optical Fabry–Pérot cavity. This configuration enables the mechanical mode to mediate energy exchange between the microwave and optical domains. When both cavities are pumped appropriately, the system realizes an effective beam-splitter-type or two-mode squeezing interaction, depending on detuning configurations, enabling quantum state transfer or entanglement generation across the frequency gap.

Figure 9 illustrates a simplified version of the proposed quantum radar architecture based on EOM transduction proposed in¹⁵, which enables coherent photon conversion between the optical and microwave domains. An entangled photon source injects optical signals into a high-fidelity optical cavity, which is mechanically coupled to a superconducting microwave cavity via a suspended membrane. This tripartite system—comprising optical, mechanical, and microwave modes—functions as a quantum transducer, converting optical photons into microwave photons via radiation-pressuremediated interactions. The generated microwave signal is transmitted toward a distant target via antenna, where it scatters and partially reflects back. In actual implementation, there is no free-space propagation; the antenna is included in the illustration only to aid conceptual understanding¹⁵. Upon reception, the microwave echo is routed into a second EOM converter, where it is upconverted to the optical domain. This returned optical signal is jointly measured with the stored idler photon using a coincidence counter, enabling quantum correlation analysis. By preserving non-classical correlations between the transmitted and received modes, this system enhances detection sensitivity in noisy environments, exemplifying the potential of hybrid transduction-based quantum radar¹⁵.

The opto-electronic (OE) quantum radar illustrated in Fig.10 employs a hybrid interface where the entangled photon pairs generated in the optical parametric downconverter (OPDC) are split into a signal and an idler. The idler photon remains in the optical domain and is stored locally as a reference, while the signal photon excites a quantum-dot photodetector. The resulting photocurrent modulates the VD, which tunes the resonance of a microwave cavity to generate microwave photons. These photons are transmitted toward the target and, after scattering and returning through a noisy channel, are detected alongside the retained idler. The detection process relies on the statistical correlation between the optical idler and the returned microwave mode, where the presence of nonclassical correlations indicates the presence of the target.

Josephson-based parametric devices are central to the implementation of microwave quantum radar systems, providing the essential functionality for entanglement generation, amplification, and frequency conversion in the cryogenic domain^{19–21}. Among these, the JPA has been extensively used as a narrowband quantum-limited amplifier capable of generating two-mode squeezed vacuum (TMSV) states by modulating a nonlinear inductance based on the Josephson effect. JPAs are typically used in early stage quantum radar prototypes, where they serve as an entangled signal-idler source in quantum illumination or quantum-enhanced noise radar schemes^{19,28}. Despite their limited bandwidth (on the order of a few MHz), JPAs offer excellent noise performance and phase-sensitive gain, making them suitable for proofof-principle demonstrations of quantum correlations at microwave frequencies 19,28.

In addition to JPA, the JPC is designed to perform both non-degenerate amplification and frequency conversion between two orthogonal microwave modes, typically referred to as signal and idler²⁰. JPCs operate via three-wave mixing and exhibit low added noise, making them especially useful in experiments that require simultaneous amplification and separation of entangled modes. They have been used in quantum illumination implementations that adopt digital receivers, where signal and idler beams are downconverted and processed electronically to extract second-order correlations²⁰. However, similar to JPAs, JPCs suffer from limited dynamic range and bandwidth.

To overcome these limitations, the JTWPA has emerged as a broadband high-gain entangled microwave source with minimal added noise⁶². Unlike cavity-based JPAs and JPCs, the JTWPA supports traveling wave propagation of microwave signals along a dispersion-engineered nonlinear transmission line, enabling squeezing and amplification over GHz-scale bandwidths. Unlike cavity-based JPAs and JPCs, the JTWPA supports traveling wave propagation of microwave signals along a dispersion-engineered nonlinear transmission line, enabling squeezing and amplification over GHz scale bandwidths⁶². This makes JTWPAs particularly well suited for scalable and long-range quantum radar architectures. In recent work, JTWPAs have been employed in a radar prototype implementing quantum illumination with a phase-conjugate receiver, allowing for enhanced detection perfor-

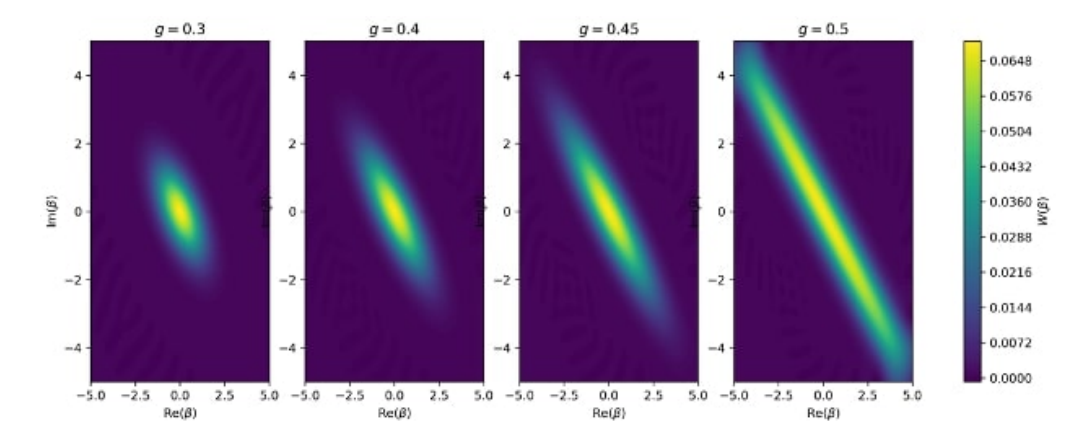


FIG. 8: Steady-state Wigner functions of a nonlinear JPA for varying parametric gain factors g. The Wigner function $W(\beta)$ is plotted in the complex phase space, showing increasing squeezing and nonclassicality as g increases from 0.3 to 0.5. The results highlight the transition of the JPA output toward a highly squeezed quantum state, suitable for entangled photon generation.

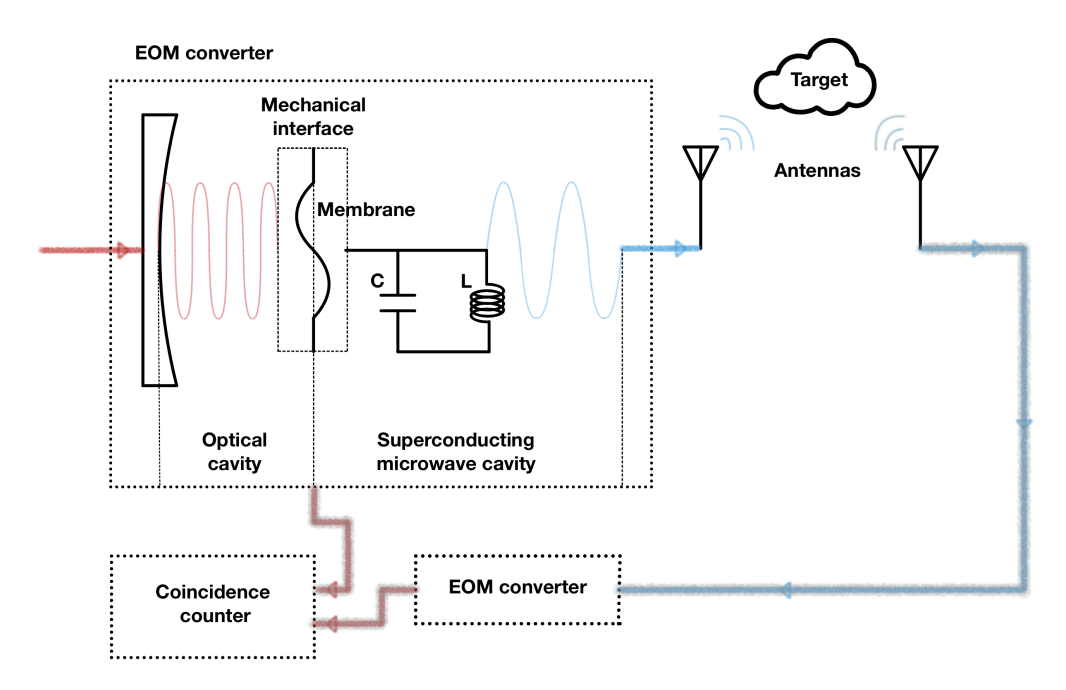


FIG. 9: Quantum radar architecture using EOM transduction for microwave-optical signal conversion¹⁵.

mance even in the presence of amplifier-induced decoherence and thermal $noise^{21}$.

The three circuit schematics illustrate the fundamental designs of Josephson-based parametric devices. Fig. 11, depicts the JPA, which consists of a lumped element LC resonator shunted by a Josephson junction (JJ) or a tunable SQUID^{19,76}. Fig. 12 shows the JPC, based on a Josephson Ring Modulator (JRM) composed of four Josephson junctions arranged in a Wheatstone bridge configuration^{15,77}. Fig. 13 presents the architecture of the JTWPA, which uses a long, dispersion-engineered nonlinear transmission line made of cascaded unit cells containing Josephson junctions and capacitive elements^{21,62,78}.

B. Atmosphere, Channel, and Related Loss

Atmospheric losses are frequency-dependent. Both radar and lidar systems often operate in frequency bands where atmospheric transmission is relatively low. In general, attenuation and scattering are less severe at microwave frequencies compared to optical frequencies. This difference becomes even more pronounced under adverse weather conditions such as rain or fog²². The atmosphere plays a crucial role in affecting quantum beams. Atmospheric losses in quantum signals can be divided into two categories: static components and dynamic components. To model atmospheric absorption and scattering effects under various conditions and across a wide wavelength range, many atmospheric radiative transfer simu-

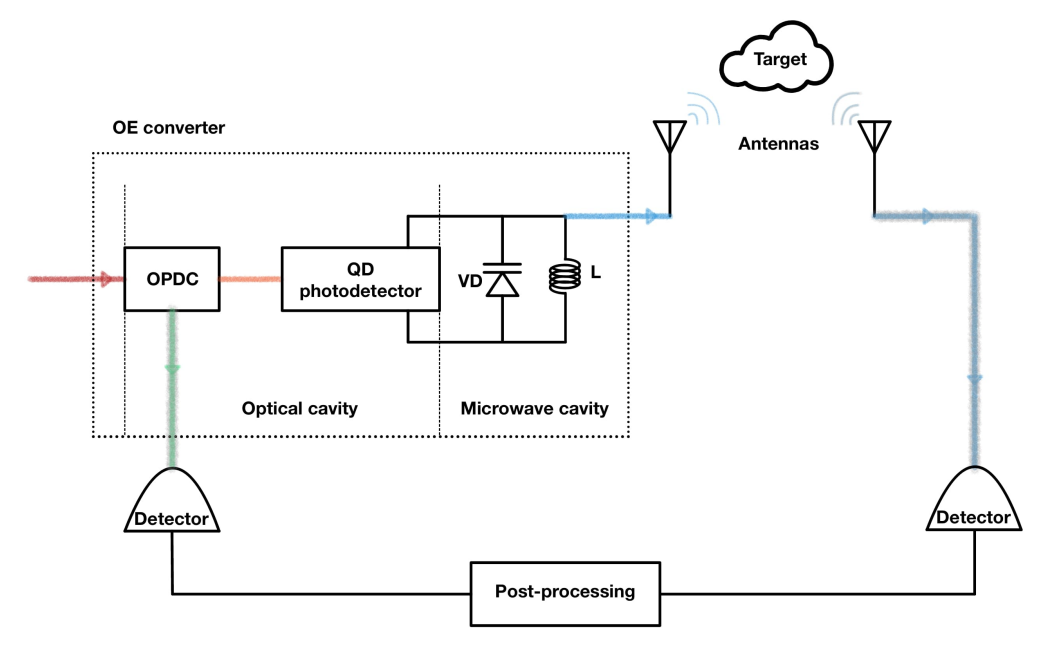


FIG. 10: Opto-electronic quantum radar with optical idler storage and microwave signal transmission⁵⁹.

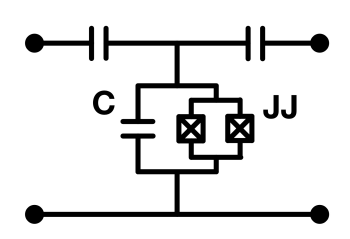


FIG. 11: The JPA consisting of a JJ or a tunable SQUID shunted to a lumped-element LC resonator 19,76.

lation tools have been developed.

Microwave photons are an effective method for connecting superconducting qubit chips in quantum communication. Although thermal noise is higher at microwave frequencies, signal loss in the atmosphere is low. The antenna impedance depends on differences between environments and can be tuned using nanofabrication techniques. Absorption losses due to superconductivity degradation along long transmission lines between cryogenic and room temperatures are modeled by an infinite series of beam splitters, whose overall effect can be represented by a single effective beam splitter. The effective number of thermal photons introduced into the system by this beam splitter:

$$n_{\text{eff}} = \frac{\int_0^L dx \, \mu(x) \, n(x) \, e^{-\int_0^x dx' \, \mu(x')}}{1 - e^{-\int_0^L dx \, \mu(x)}}$$
(31)

This expression is general and can be applied to any situation where the temperature profile is known. Let's choose a simple but useful profile that will allow us to obtain a closed-form expression. If we assume that a length L can be kept

below the critical temperature, then we can make the following choice:

$$n(x) = n(T_{\rm in}) + [n(T_{\rm out}) - n(T_{\rm in})]\theta(x - L_0),$$
 (32)

$$\mu(x) = \mu_{\text{in}} + (\mu_{\text{out}} - \mu_{\text{in}})\theta(x - L_0),$$
 (33)

Here, μ in defines the absorption losses at cryogenic temperatures, while μ out represents the material-related absorption losses at room temperature. In this case, the effective number of thermal photons introduced into the system is as follows:

$$n_{\text{eff}} = n(T_{\text{in}}) \frac{e^{-\mu_{\text{out}}(L-L_0)}(1 - e^{-\mu_{\text{in}}L_0})}{1 - e^{-\mu_{\text{in}}L_0}e^{-\mu_{\text{out}}(L-L_0)}} + n(T_{\text{out}}) \frac{1 - e^{-\mu_{\text{out}}(L-L_0)}}{1 - e^{-\mu_{\text{in}}L_0}e^{-\mu_{\text{out}}(L-L_0)}}$$
(34)

Quantum entanglement is a key resource for many quantum information applications, but it is fragile and can easily be destroyed by interactions with the environment, known as quantum decoherence. Entanglement is a highly delicate and unstable state. Therefore, creating and maintaining entangled states is quite challenging. Environmental effects, especially thermal noise, can easily disrupt these states²³. One of the most common issues encountered in quantum radar systems is the propagation of entangled microwave photons through the atmosphere to detect the target. However, since the atmosphere exhibits attenuating effects, the signal generated by the target becomes significantly weakened²⁴. Factors such as temperature, pressure, and the interaction of light with solid particles in free space cannot be controlled. Hence, temperature is a particularly critical factor, as thermal photons present in the environment can interact with low-energy entangled photons and disrupt the entanglement. For this reason, entangled photons must be generated at very low temperatures. As the

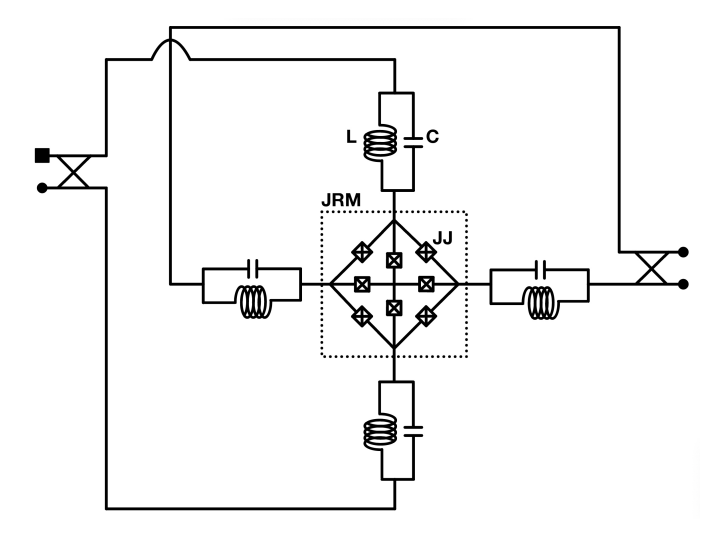


FIG. 12: The JPC based on a JRM composed of four Josephson junctions arranged in a Wheatstone bridge configuration 15,77.

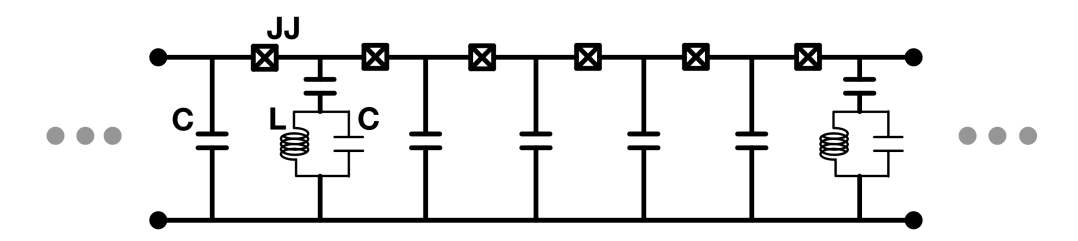


FIG. 13: The JTWPA composed of a cascaded array of unit cells containing Josephson junctions and capacitive elements ^{21,62,78}.

number of thermal photons in the environment increases, entanglement becomes more susceptible to degradation. Consequently, in related studies, the operating temperature is generally kept limited.

After the entangled microwave photons are generated, they are transmitted through the atmosphere to detect the target. To investigate the effects of the atmosphere on these photons, attenuating environments and reflections from the target have been theoretically modeled using beam splitters²⁶. Within the framework of quantum mechanics, these effects have been analyzed by considering the atmosphere as a system composed of sequential beam splitters²⁵. Each beam splitter receives the incoming signal and thermal photons from one side and outputs the desired signal along with environment-induced noise from the other side. The amount of thermal photons present in the environment varies depending on the temperature and altitude of the atmosphere. When entangled photons propagate through the atmosphere, these interactions can significantly weaken the entanglement between the modes.

When examining the scattering effect from the target, the

signals propagating through the atmosphere contain both entangled and separable (non-entangled) photons. Depending on atmospheric conditions, the number of entangled photons reaching the target varies. Therefore, the signals interacting with the field generated by the target atom may consist of both entangled and separable photons. This interaction has been modeled using a sequence of beam splitters, where the input corresponds to signals containing thermal photons and the output corresponds to the scattered photons.

The atmospheric environment is considered as a structure containing scattering centers. These centers are represented using beam splitters within a quantum electrodynamics framework²⁶. The modeling process begins with the scattering effects in the attenuating medium. For the j-th beam splitter, the inputs are defined as c_{awj} , b_j , and the outputs as $c_{aw(j+1)}$, a_{sj} . Therefore, the attenuating medium can be described by a continuous model using a complex coupling coefficient. This model satisfies the condition $|t(\omega)|^2 + |r(\omega)|^2 = 1$, where $t(\omega)$ represents the transmission coefficient and $r(\omega)$ denotes the reflection coefficient²⁶.

$$\hat{c}_{a}(\boldsymbol{\omega}) = e^{[jk_{\text{atm}} - \kappa_{\text{atm}}(\boldsymbol{\omega})]R} \hat{c}_{w}(\boldsymbol{\omega}) + j\sqrt{2\kappa_{\text{atm}}(\boldsymbol{\omega})} \int_{0}^{R} dz e^{[jk_{\text{atm}} + \kappa_{\text{atm}}(\boldsymbol{\omega})](R-z)} \hat{b}(\boldsymbol{\omega}, z)$$
(35)

 $c_a(\omega)$, K_{atm} , and $K_{\text{atm}}(\omega)$ represent the attenuation medium

output mode operator, the real component of the wave vector,

and the imaginary component of the wave vector, respectively. As illustrated in Fig.14, the impact of the atmospheric attenuation medium on microwave cavity modes is modeled using beam splitter techniques.

Another significant factor in quantum radar is the reflection of the signal from the target. This effect can disrupt entangled states. Similar to the approach used for the attenuating medium, quantum electrodynamics theory is employed here to model the scattering effect. In the quantum framework, reflection from the target is defined as scattering occurring from the target atoms. This process represents the interaction between the electromagnetic quantum field and the quantum fields of the atoms in the target. Thermal photons play a particularly important role during scattering, exerting substantial influence on entanglement. To model this process, the j-th beam splitter (BS) is considered as a reflective element. In this case, the relationship between the input and output is continuously defined as follows²⁶:

$$\hat{c}_{t}(\boldsymbol{\omega}) = \left[t(\boldsymbol{\omega}) e^{iK_{t}\Delta z_{t}} + 2\kappa_{t}(\boldsymbol{\omega}) \sqrt{\Delta z_{t}} \int_{0}^{z_{t}} dz \left\{ t(\boldsymbol{\omega}) e^{[iK_{t} - \kappa_{t}(\boldsymbol{\omega})]} \right\}^{(z_{t} - z)} \right] \hat{c}_{a}(\boldsymbol{\omega})$$

$$+ i\sqrt{\kappa_{t}(\boldsymbol{\omega})\Delta z_{t}} e^{[iK_{t} - \kappa_{t}(\boldsymbol{\omega})]z_{t}} \hat{b}_{t}(\boldsymbol{\omega})$$
(36)

where $c_t(\omega)$, K_t , and $\kappa_t(\omega)$ denote the target's scattering output mode operator, the real part of the wave vector, and the imaginary part of the wave vector, respectively. The first term in Eq.36 represents the effect of the imaginary part of the target's dielectric constant. The second term reflects the influence of thermally excited photons. In other words, Eq.36 indicates a significant reduction in the amplitude of the incoming wave, denoted as $c_a(\omega)$. More importantly, the phase information caused by the thermal photons in the second term of Eq.36 can severely disrupt the entanglement. Fig.15 illustrates the modeling of target scattering using beam splitter techniques.

Photons reflected from the target propagate again through the atmosphere. Therefore, to complete the quantum radar process, the effect of the atmosphere must be considered once more. However, there is a significant difference here: while the input signal initially entering the atmosphere contains a substantial number of entangled photons, the photons reflected from the target typically lose their entanglement. This makes the atmosphere's impact on entanglement even more critical. As depicted in Fig.16, the transmission of the scattered signal through the atmosphere, treated as an attenuation medium, is represented using beam splitter techniques. Consequently, the system must be designed so that the entanglement is not completely disrupted by external effects, such as atmospheric attenuation and scattering from the target²⁶.

The effects of atmospheric and target scattering have been examined using Eq. 35 and Eq. 36. Although these effects are uncontrollable, suitable systems can be designed to generate entangled states at high temperatures. Thus, the harmful impacts of atmospheric and target scattering can be mitigated, preserving entanglement.

In this study, the effects of the attenuating medium, target scattering, backscattered photons, and atmospheric propagation modes on entanglement were investigated at various distances between the receiver and transmitter. According to Eq. 35 and Eq. 36, as the distance between the transmitter and receiver increases, the number of thermally excited photons increases significantly. This leads to a reduction in the entanglement between the modes.

However, in terms of path loss, because of its proximity to Earth, a low Earth orbit (LEO) experiences minimal diffraction loss, making it particularly useful for quantum key distribution (QKD) experiments. On the other hand, orbits like middle Earth orbit (MEO) and geosynchronous Earth orbit (GEO) have slower speeds that enable maintaining continuous connections for longer periods, supporting extended QKD operations. However, MEO and GEO also present challenges, such as higher radiation levels and increased propagation losses, that need to be considered. If examined in terms of turbulence, the structure constant C_n^2 is a common parameter used to describe wave propagation in random media such as the atmosphere. This constant quantifies fluctuations in the refractive index n caused by irregularities within the medium. To accurately model the atmosphere, it is important to understand how the structure constant varies with altitude and responds to different weather conditions. Performing a precise model of the atmosphere is challenging, and various empirical and parametric models have been developed to describe how C_n^2 changes with height. Some commonly used atmospheric models include the Hufnagel-Valley (H-V) model, the Polynomial Regression (PR) model, and the Submarine Laser Communication (SLC) model. Among these, the H-V model is the most widely adopted.

Due to atmospheric turbulence, the beam also experiences increased divergence. To manage this, an aperture size of 15 cm has been chosen as optimal. Smaller apertures result in higher transmission losses, while larger apertures are more susceptible to turbulence, leading to a lower Strehl ratio at the detector. To further enhance performance, additional technologies such as Adaptive Optics (AO) can be implemented. Another major source of loss is atmospheric absorption. This issue has previously been addressed in discussions on quantum interferometric radar. Although adaptive optics can also help mitigate this problem, their use is similarly subject to practical limitations and constraints⁸⁰.

Studies in this direction can be summarized as follows.

In certain system configurations, the impact of thermal noise on the antenna can be significantly reduced by incorporating cryogenic losses prior to the antenna input^{81,82}. In-

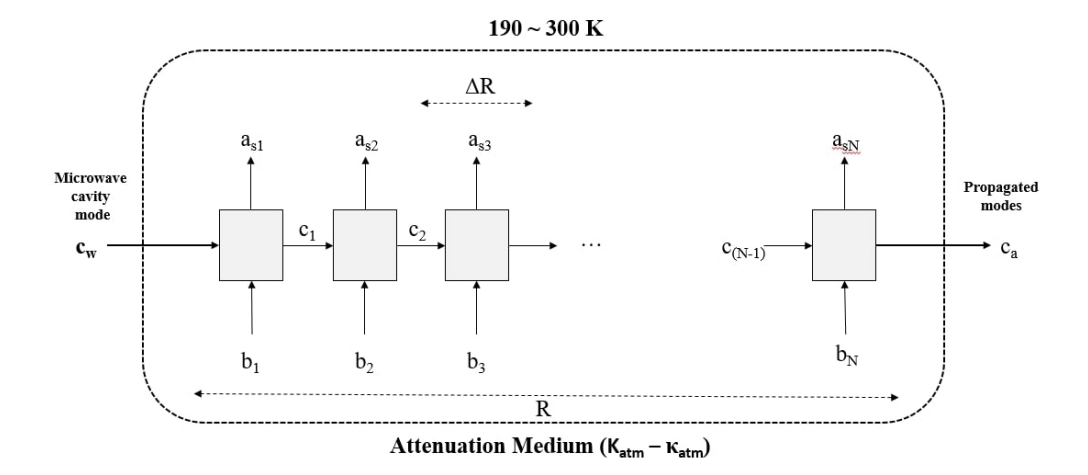


FIG. 14: Modeling the impact of the atmospheric attenuation medium on microwave cavity modes through beam splitter techniques⁷⁹.

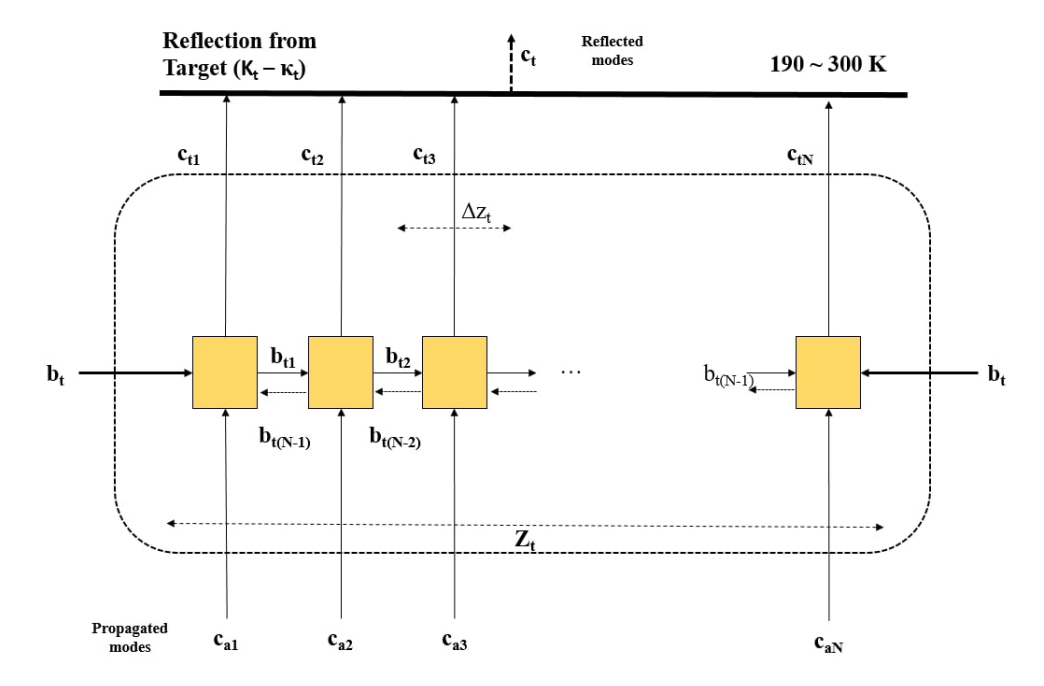


FIG. 15: Target scattering modeled through beam splitter techniques⁷⁹.

stead of assuming that thermal photons enter directly through the antenna, some are absorbed within the cryostat, effectively lowering the thermal noise contribution. Including these losses creates a trade-off between the entanglement degradation introduced by the effective beam splitter and the improved antenna performance due to a reduced thermal photon population. This balance is highly sensitive to the temperature profile along the transmission line, which must be accurately characterized to inform subsequent impedance optimization and modeling of entanglement loss beyond the antenna^{81,82}.

Recent studies have demonstrated that entanglement-based quantum communication protocols can enable secure transmission even under high-loss and noisy conditions. For instance, the first experimental implementation of a protocol that maintains secure communication despite channel noise exceeding the entanglement-breaking threshold by 8.3 dB was reported in²⁷. This protocol relies on interference, requiring precise timing between the signal and idler paths, and employs dispersion- compensating fiber to maintain performance. Despite a total measured channel loss of approximately 16.4 dB and an idler loss of 4.1 dB, the system successfully sustained secure communication. These results highlight the practical feasibility of entanglement-based quantum communication in realistic, lossy, and noisy fiber-optic environments²⁷.

Nonclassical states are fundamental to optical quantum information processing, but their fragility limits their practical use since loss and noise inevitably degrade or destroy their quantum properties. In quantum metrology, nonclassical states offer sensitivity advantages over all classical systems using the same probe energy. However, these improvements are almost always severely reduced by quantum decoherence. In⁷, an entanglement-enhanced sensing system that remains robust against decoherence is experimentally demonstrated. Despite facing 14 dB loss and a noise background 75 dB stronger than the returned signal, conditions that typically destroy entanglement, a 20 percent improvement in SNR compared to the best classical system has been achieved. This result suggests that quantum sensing technologies can offer practical advantages under noisy and lossy conditions⁷. The performance advantage of QI over classical illumination (CI) with the same probe energy arises from the strong correlations between the returned and stored beams created by the initial entanglement, even when the environment destroys the entanglement itself. Joint measurement leverages this strong quantum signature to outperform classical systems. Here, missing experimental evidence that QI can significantly improve target detection performance compared to the best classical system under conditions that destroy entanglement is provided⁷. Measured SNR values for QI closely match theoretical predictions, while classical illumination SNR deviates slightly at the lowest and highest transmission values due to polarization drifts and laser phase instability, respectively. The QI system's SNR advantage holds despite the channel completely destroying the initial signal-idler entanglement, indicating that the initial quantum correlations still provide measurable benefits. This shows that entanglement-based protocols can improve sensing performance under harsh conditions where traditional thinking expects quantum advantages to vanish⁷. In summary, the authors implement an entanglement-based sensing protocol that enhances SNR over optimal classical systems even in environments with high loss and strong noise that fully eliminate initial entanglement. Achieving this quantum advantage without compensating for device imperfections challenges the conventional view that quantum benefits disappear under such conditions and motivates further exploration of quantum information techniques for practical applications⁷.

Satellite-based quantum communication, particularly quantum key distribution (QKD), is considered a key enabler for global quantum networks⁸³. To assess the feasibility of such systems, realistic atmospheric simulations are realized—especially for uplink scenarios where the quantum signal interacts with the atmosphere early in its propagation⁸³. A study in⁸³ validated its simulation methodology using experimental data from the Canary Islands and Canada, and applied it to evaluate three ground stations in India. Through atmospheric modeling and link budget analysis, the study identified IAO Hanle as the most suitable site for uplink-based quantum communication among the considered locations⁸³.

In the absence of atmospheric turbulence, the received power at the satellite detector is mainly affected by free-space path loss and optical absorption. Taking into account optical losses in both the transmitter and receiver components, as well as atmospheric absorption, the received power can be calculated accordingly⁸³.

C. Quantum Receiver

In microwave quantum illumination, the quantum receiver is central to extracting performance gains over classical radar systems. The ideal quantum receiver performs a joint measurement between the returned signal and the retained idler mode, leveraging quantum correlations, such as entanglement or squeezing, to discriminate the presence or absence of a target in high noise⁵. However, realizing such optimal joint measurements at microwave frequencies remains technologically difficult due to the absence of practical quantum memories⁸⁴, single-photon detectors⁸⁵, and loss in cryogenic microwave transmission⁸⁶.

To overcome these limitations, researchers have developed classically assisted receiver architectures that approximate quantum advantages without requiring ideal quantum hardware. For example, in a proof-of-principle experiment using the JPC, signal and idler beams are downconverted, digitized, and then post-processed classically to evaluate their second-order quadrature correlations²⁰. This so-called digital receiver allows partial recovery of the quantum illumination benefit, even though it does not implement an entanglement-preserving joint detection. The trade-off is a suboptimal but implementable receiver that can still outperform the classical radar in terms of error probability or receiver operating characteristics.

In practice, the receiver chain integrates a hierarchy of amplifiers in multiple temperature stages. Mostly, started by high-electron-mobility transistors (HEMTs) at the 4 K stage and low-noise amplifiers (LNAs) at room temperature.

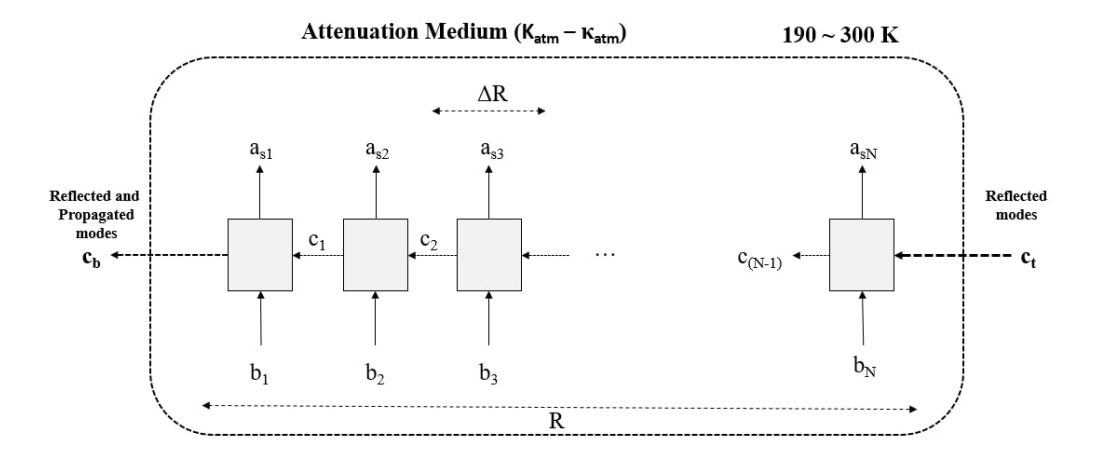


FIG. 16: Representation of scattering signal transmission through the atmosphere as an attenuation medium via beam splitters⁷⁹.

This sequential chain guarantees the preservation of delicate quantum correlations encoded in the weak microwave signals throughout the amplification process, enabling accurate digitization. The reflected signal, collected by a secondary antenna, is downconverted through an IQ mixer driven by a local oscillator, producing in-phase (I) and quadrature (Q) components. These signals are digitized and stored for correlation analysis with the retained idler, enabling quantum-enhanced detection without the need for optical quantum memories. This hybrid design, which combines cryogenic amplification and classical digital processing, makes the quantum receiver both scalable and robust to loss, thereby bridging theoretical proposals with experimental feasibility in quantum radar.

Other strategies, such as quantum-enhanced noise radar, use TMSV states generated by JPAs, but forego direct joint measurement¹⁹. Instead, they rely on statistical analysis of the correlations between noisy return signals and stored idler beams, again evaluated digitally.

D. Quantum Signal Processing and FPGA

Quantum signal processing in microwave quantum radar systems is fundamentally based on analyzing the statistical structure of quadrature measurements from the *signal* and *idler* fields generated via the TMSV states. These states are modeled using Gaussian quantum optics, which allows complete characterization via covariance matrices of the field quadratures⁸⁷.

The quadrature operators for the signal (\hat{a}_s) and idler (\hat{a}_i) modes are defined as:

$$\hat{x}_k = \frac{1}{\sqrt{2}} \left(\hat{a}_k + \hat{a}_k^{\dagger} \right), \quad \hat{p}_k = \frac{-j}{\sqrt{2}} \left(\hat{a}_k - \hat{a}_k^{\dagger} \right)$$
 (37)

where k = s, i denotes the signal and idler, respectively.

The 4×4 covariance matrix **V** for the joint Gaussian state of signal and idler is defined by:

$$V_{mn} = \frac{1}{2} \left\langle \{\hat{\xi}_m, \hat{\xi}_n\} \right\rangle - \left\langle \hat{\xi}_m \right\rangle \left\langle \hat{\xi}_n \right\rangle \tag{38}$$

with the quadrature vector:

$$\hat{\xi} = (\hat{x}_s, \hat{p}_s, \hat{x}_i, \hat{p}_i)^T \tag{39}$$

For an ideal TMSV state with squeezing parameter r, the covariance matrix takes the standard form:

$$\mathbf{V}_{\text{TMSV}} = \begin{bmatrix} \cosh(2r) \, \mathbb{I}_2 & \sinh(2r) \, \sigma_z \\ \sinh(2r) \, \sigma_z & \cosh(2r) \, \mathbb{I}_2 \end{bmatrix} \tag{40}$$

where $\sigma_z = \text{diag}(1, -1)$ and \mathbb{I}_2 is the 2×2 identity matrix⁸⁸.

In a quantum radar receiver, these quadratures are sampled using heterodyne or homodyne detection. After the signal interacts with the environment and reflects back, it is combined

with the stored idler (or a digitally processed replica) to compute second-order moments and perform detection.

The quantum correlation coefficient ρ between the signal and idler is often extracted from the off-diagonal terms of the covariance matrix:

$$\rho = \frac{\text{Cov}(x_s, x_i)}{\sqrt{\text{Var}(x_s)\text{Var}(x_i)}}$$
(41)

This coefficient directly influences the Receiver Operating Characteristic (ROC) curves and the detection performance^{87,88}.

The quantum receiver architecture replaces the ideal joint quantum measurement with a classical post-processed measurement scheme, enabled by high-speed analog-to-digital converters (ADC)²⁰. Both the retained idler and the reflected signal are amplified and downconverted to an intermediate frequency, then sampled by high-resolution ADCs operating at 1 GS/s (giga-sample per second). These ADCs capture the in-phase (I) and quadrature (Q) components of each field with sufficient temporal resolution to retain the underlying quantum correlations²⁰. These ADCs capture the I and Q components of each field with sufficient temporal resolution to retain the underlying quantum correlations. The sampled I and Q data are first transferred to a field-programmable gate array (FPGA) embedded on the digitizer board, where initial data buffering and formatting are performed. Subsequently, the data is sent to a host PC for further digital post-processing.

In the host PC, the digitized I/Q data streams are processed using a correlation-based digital receiver implemented in software^{20,89–91}. The receiver computes second-order moments (e.g., covariance between signal and idler quadratures) to estimate the presence or absence of a target. This digital postprocessing step substitutes for a true quantum joint measurement, enabling a practical and scalable realization of quantum illumination in the microwave domain.

IV. MICROWAVE QUANTUM RADAR EXPERIMENTAL SYSTEMS

In microwave quantum radar systems, achieving reliable detection of weak signals requires high-sensitivity and lownoise amplification. In this context, various amplifier technologies operating at different temperature stages are combined to amplify and preserve quantum-correlated signals. Particularly, HEMT amplifiers operating at the 4 K temperature stage play a critical role in practical implementations. Below, a typical amplification and signal processing architecture used in microwave quantum radar experiments is detailed, with an emphasis on the role of HEMT amplifiers within the system. Figure 17 illustrates a typical cryogenic measurement and signal acquisition architecture for microwave quantum radar experiments^{20,28}. The setup integrates quantumlimited amplification, low-noise detection, and high-speed digital signal processing to facilitate quantum-enhanced microwave sensing.

At the heart of the system lies the JPA, JPC, or JTWPA operating at 10 mK, accommodated inside a dilution refriger-

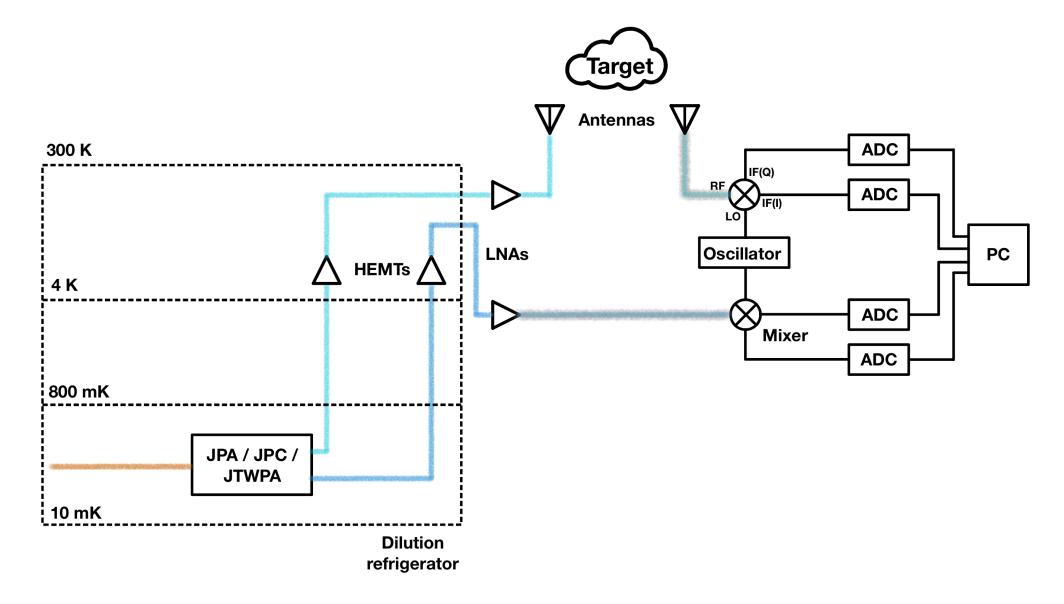


FIG. 17: Experimental setup.

ator. These superconducting quantum devices generate and amplify entangled microwave signal-idler pairs at quantumlimited noise levels.

The outgoing microwave signal travels through multiple temperature stages, passing through HEMT amplifiers at the 4 K stage and low-noise amplifiers (LNAs) at room temperature (300 K) to boost signal strength while preserving phasesensitive correlations. The signal is then transmitted through the horn antennas toward a target, where weak reflection is expected.

At the 4 K stage, this amplification is carried out by HEMT amplifiers, which are widely used cryogenic devices in microwave quantum sensing and quantum radar systems. HEMTs have very high carrier mobility and low-noise performance at gigahertz frequencies⁹². While parametric amplifiers at millikelvin stages provide near-quantum-limited gain, HEMTs deliver the secondary amplification necessary to boost weak microwave signals for further processing at room temperature. Although their noise temperature—typically a few kelvin—is higher than that of superconducting amplifiers, HEMTs remain critical for preserving the fragile information carried by entangled or correlated microwave photons, making them indispensable for practical quantum radar implementations.

The reflected signal is received by a second antenna and downconverted using an IQ mixer driven by a local oscillator (LO), producing two intermediate frequency (IF) channels: in-phase (I) and quadrature (Q). These analog signals are then digitized using high-speed ADCs. The digitized I and Q data are routed to a host PC for digital postprocessing, where signal-idler correlations are extracted using second-order moment analysis to determine target presence.

This setup enables the evaluation of quantum illumination protocols without requiring optical quantum memory, making it scalable and more robust to loss.

V. CONCLUSION

This review has provided a comprehensive examination of microwave quantum radar, spanning from its foundational theoretical principles to the practical challenges and advances in real-world implementations. We began by discussing quantum illumination protocols and the critical role of entanglement in enhancing detection sensitivity beyond classical limits, even in highly lossy and noisy environments. The generation of entangled microwave photon pairs via superconducting devices such as JPAs, JPCs, and JTWPAs at millikelvin temperatures was highlighted as a key enabling technology.

Subsequent sections detailed the architecture of quantum radar subsystems, including quantum receivers that leverage high-speed analog-to-digital converters and classical post-processing to approximate optimal quantum measurements. The integration of cryogenic amplifiers, such as HEMTs and LNAs, plays a vital role in preserving fragile quantum correlations during signal transmission and reflection.

Furthermore, the review addressed environmental effects such as atmospheric attenuation, turbulence, and target scattering, which pose significant challenges to maintaining entanglement over practical distances. Modeling these effects via beam splitter techniques and incorporating empirical atmospheric models provides critical insights for system design and optimization. Notably, experimental demonstrations have shown that quantum radar protocols can maintain performance advantages under realistic operational conditions, including high loss and strong thermal noise that completely degrade initial entanglement. These findings underscore that initial quantum correlations, even when destroyed by the environment, can still be exploited via joint detection or correlation-based digital receivers to outperform classical radar systems in signal-to-noise ratio and detection sensitivity.

Looking forward, significant technical challenges remain,

including the development of scalable quantum memories, low-noise single-photon detectors in the microwave regime, and integrated optoelectronic interfaces. Nonetheless, the steady progress in superconducting device engineering, cryogenic amplification, and advanced digital signal processing points towards the practical realization of microwave quantum radar systems. Moreover, satellite-based quantum communication experiments and atmospheric channel simulations illustrate the feasibility of global quantum networks that can benefit from quantum radar and sensing technologies.

In conclusion, microwave quantum radar stands as a promising frontier that bridges fundamental quantum physics with applied sensing technologies, offering new paradigms in detection performance, robustness, and applications extending from secure communication to environmental monitoring. Continued interdisciplinary research and technological innovation will be essential to unlock the full potential of quantum radar in both terrestrial and space-based platforms.

- ¹S. Lloyd, "Enhanced sensitivity of photodetection via quantum illumination," Science **321**, 1463–1465 (2008).
- ²M. I. Skolnik et al., Introduction to radar systems, Vol. 3 (McGraw-hill New York, 1980).
- ³S.-H. Tan, B. I. Erkmen, V. Giovannetti, S. Guha, S. Lloyd, L. Maccone, S. Pirandola, and J. H. Shapiro, "Quantum illumination with gaussian states," Physical review letters **101**, 253601 (2008).
- ⁴J. H. Shapiro, "The quantum illumination story," IEEE Aerospace and Electronic Systems Magazine **35**, 8–20 (2020).
- ⁵S. Guha and B. I. Erkmen, "Gaussian-state quantum-illumination receivers for target detection," Physical Review A—Atomic, Molecular, and Optical Physics **80**, 052310 (2009).
- ⁶E. Lopaeva, I. Ruo Berchera, I. P. Degiovanni, S. Olivares, G. Brida, and M. Genovese, "Experimental realization of quantum illumination," Physical review letters **110**, 153603 (2013).
- ⁷Z. Zhang, S. Mouradian, F. N. Wong, and J. H. Shapiro, "Entanglement-enhanced sensing in a lossy and noisy environment," Physical review letters **114**, 110506 (2015).
- ⁸D. G. England, B. Balaji, and B. J. Sussman, "Quantum-enhanced standoff detection using correlated photon pairs," Physical Review A **99**, 023828 (2019)
- ⁹H. Liu, D. Giovannini, H. He, D. England, B. J. Sussman, B. Balaji, and A. S. Helmy, "Enhancing lidar performance metrics using continuous-wave photon-pair sources," Optica 6, 1349–1355 (2019).
- ¹⁰J. Zhao, A. Lyons, A. C. Ulku, H. Defienne, D. Faccio, and E. Charbon, "Light detection and ranging with entangled photons," Optics Express 30, 3675–3683 (2022).
- ¹¹ A. Serafini, "Detecting entanglement by symplectic uncertainty relations," Journal of the Optical Society of America B 24, 347–354 (2007).
- ¹²R. Simon, "Peres-horodecki separability criterion for continuous variable systems," Physical Review Letters 84, 2726 (2000).
- ¹³H. Ollivier and W. H. Zurek, "Quantum discord: a measure of the quantumness of correlations," Physical review letters 88, 017901 (2001).
- ¹⁴L. Henderson and V. Vedral, "Classical, quantum and total correlations," Journal of physics A: mathematical and general 34, 6899 (2001).
- ¹⁵S. Barzanjeh, S. Guha, C. Weedbrook, D. Vitali, J. H. Shapiro, and S. Pirandola, "Microwave quantum illumination," Physical review letters 114, 080503 (2015).
- ¹⁶S. Barzanjeh, M. Abdi, G. J. Milburn, P. Tombesi, and D. Vitali, "Reversible optical-to-microwave quantum interface," Physical Review Letters 109, 130503 (2012).
- ¹⁷J. D. Teufel, D. Li, M. S. Allman, K. Cicak, A. Sirois, J. D. Whittaker, and R. Simmonds, "Circuit cavity electromechanics in the strong-coupling regime," Nature 471, 204–208 (2011).
- ¹⁸ A. Salmanogli, D. Gokcen, and H. S. Gecim, "Entanglement of optical and microcavity modes by means of an optoelectronic system," Physical Review Applied 11, 024075 (2019).

- ¹⁹C. Chang, A. Vadiraj, J. Bourassa, B. Balaji, and C. Wilson, "Quantum-enhanced noise radar," Applied Physics Letters 114 (2019).
- ²⁰S. Barzanjeh, S. Pirandola, D. Vitali, and J. M. Fink, "Microwave quantum illumination using a digital receiver," Science advances 6, eabb0451 (2020).
- ²¹P. Livreri, E. Enrico, L. Fasolo, A. Greco, A. Rettaroli, D. Vitali, A. Farina, C. F. Marchetti, and A. S. D. Giacomin, "Microwave quantum radar using a josephson traveling wave parametric amplifier," in 2022 IEEE Radar Conference (RadarConf22) (IEEE, 2022) pp. 1–5.
- ²²M. Höijer, T. Hult, and P. Jonsson, "Quantum radar–a survey of the science, technology and literature," Swedish Defence Research Agency, Tech. Rep. FOI (2019).
- ²³A. Salmanogli, "Modification of a plasmonic nanoparticle lifetime by coupled quantum dots," Physical Review A 100, 013817 (2019).
- ²⁴A. Salmanogli and D. Gokcen, "Analysis of quantum radar cross-section by canonical quantization method (full quantum theory)," Ieee Access 8, 205487–205494 (2020).
- ²⁵J. Jeffers, N. Imoto, and R. Loudon, "Quantum optics of traveling-wave attenuators and amplifiers," Physical Review A 47, 3346 (1993).
- ²⁶A. Salmanogli and D. Gokcen, "Optoelectronic based quantum radar: Entanglement sustainability improving at high temperature," arXiv preprint arXiv:2007.10670 (2020).
- ²⁷Z. Zhang, M. Tengner, T. Zhong, F. N. Wong, and J. H. Shapiro, "Entanglement's benefit survives an entanglement-breaking channel," Physical review letters 111, 010501 (2013).
- ²⁸D. Luong, C. S. Chang, A. Vadiraj, A. Damini, C. M. Wilson, and B. Balaji, "Receiver operating characteristics for a prototype quantum two-mode squeezing radar," IEEE Transactions on Aerospace and Electronic Systems 56, 2041–2060 (2019).
- ²⁹ A. Einstein, B. Podolsky, and N. Rosen, "Can quantum-mechanical description of physical reality be considered complete?" Physical review 47, 777 (1935).
- ³⁰E. Schrödinger, "Discussion of probability relations between separated systems," Mathematical Proceedings of the Cambridge Philosophical Society 31, 555–563 (1935).
- ³¹M. A. Nielsen and I. L. Chuang, Quantum computation and quantum information (Cambridge university press, 2010).
- ³²J. S. Bell, "On the einstein podolsky rosen paradox," Physics Physique Fizika 1, 195 (1964).
- ³³M. E. Tasgin, "Measuring nonclassicality of single-mode systems," Journal of Physics B: Atomic, Molecular and Optical Physics 53, 175501 (2020).
- ³⁴W. Ge, M. E. Tasgin, and M. S. Zubairy, "Conservation relation of nonclassicality and entanglement for gaussian states in a beam splitter," Physical Review A 92, 052328 (2015).
- ³⁵A. Salmanogli, "Entangled microwave photons generation using cryogenic low noise amplifier (transistor nonlinearity effects)," Quantum Science and Technology 7, 045026 (2022).
- ³⁶A. Salmanogli, "Enhancing quantum correlation at zero-if band by confining the thermally excited photons: Inp hemt circuitry effect," Optical and Quantum Electronics 55, 745 (2023).
- ³⁷A. Peres, "Separability criterion for density matrices," Physical Review Letters 77, 1413 (1996).
- ³⁸M. Horodecki, P. Horodecki, and R. Horodecki, "Separability of mixed states: necessary and sufficient conditions," Physics Letters A 223, 1–8 (1996)
- ³⁹L.-M. Duan, G. Giedke, J. I. Cirac, and P. Zoller, "Inseparability criterion for continuous variable systems," Physical review letters 84, 2722 (2000).
- ⁴⁰P. Giorda and M. G. Paris, "Gaussian quantum discord," Physical review letters 105, 020503 (2010).
- ⁴¹G. Adesso and A. Datta, "Quantum versus classical correlations in gaussian states," Physical review letters **105**, 030501 (2010).
- ⁴²R. W. Andrews, R. W. Peterson, T. P. Purdy, K. Cicak, R. W. Simmonds, C. A. Regal, and K. W. Lehnert, "Bidirectional and efficient conversion between microwave and optical light," Nature physics 10, 321–326 (2014).
- ⁴³A. H. Safavi-Naeini and O. Painter, "Proposal for an optomechanical traveling wave phonon–photon translator," New Journal of Physics 13, 013017 (2011).
- ⁴⁴M. Aspelmeyer, T. J. Kippenberg, and F. Marquardt, "Cavity optomechanics," Reviews of Modern Physics 86, 1391–1452 (2014).
- ⁴⁵B. Huttner and S. M. Barnet, "Quantization of the electromagnetic field in dielectrics," Physical Review A 46, 4306 (1992).

- ⁴⁶A. Salmanogli and H. S. Geçim, "Optical and microcavity modes entanglement by means of plasmonic opto-mechanical system," IEEE Journal of Selected Topics in Quantum Electronics 26, 1–10 (2020).
- ⁴⁷ A. Salmanogli, D. Gokcen, and H. S. Gecim, "Entanglement sustainability in quantum radar," IEEE Journal of Selected Topics in Quantum Electronics 26, 1–11 (2020).
- ⁴⁸N. Aggarwal, K. Debnath, S. Mahajan, A. B. Bhattacherjee, and M. Mohan, "Selective entanglement in a two-mode optomechanical system," International Journal of Quantum Information 12, 1450024 (2014).
- ⁴⁹ A. Salmanogli and D. Gokcen, "Design of quantum sensor to duplicate european robins navigational system," Sensors and Actuators A: Physical 322, 112636 (2021).
- ⁵⁰S. Barzanjeh, D. Vitali, P. Tombesi, and G. Milburn, "Entangling optical and microwave cavity modes by means of a nanomechanical resonator," Physical Review A—Atomic, Molecular, and Optical Physics 84, 042342 (2011).
- ⁵¹D. Vitali, S. Gigan, A. Ferreira, H. Böhm, P. Tombesi, A. Guerreiro, V. Vedral, . f. A. Zeilinger, and M. Aspelmeyer, "Optomechanical entanglement between a movable mirror and a cavity field," Physical review letters 98, 030405 (2007).
- ⁵²Y. Shih, "Entangled photons," IEEE Journal of selected topics in quantum electronics 9, 1455–1467 (2003).
- ⁵³A. Salmanogli, "Raman mode non-classicality through entangled photon coupling to plasmonic modes," Journal of the Optical Society of America B 35, 2467–2477 (2018).
- ⁵⁴M. J. Brandsema, R. M. Narayanan, and M. Lanzagorta, "Theoretical and computational analysis of the quantum radar cross section for simple geometrical targets," Quantum Information Processing 16, 32 (2017).
- 55N. Corporation, "Battery biased fiber-optic detectors," https://www.newport.com/f/biased-fiberâăSoptic-detectors (2024), [Online; accessed 2025-08-06].
- ⁵⁶Skyworks, "Smv1702-0111f hyperabrupt junction tuning varactor," https://www.skyworksinc.com/-/media/72C2A94932044D1DB38D50B0754842F4.pdf (2020), [Online; accessed 2025-08-06].
- ⁵⁷M. O. Scully and M. S. Zubairy, *Quantum optics* (Cambridge university press, 1997).
- ⁵⁸N. Lauk, N. Sinclair, S. Barzanjeh, J. P. Covey, M. Saffman, M. Spiropulu, and C. Simon, "Perspectives on quantum transduction," Quantum Science and Technology 5, 020501 (2020).
- ⁵⁹A. Salmanogli and D. Gokcen, "Entanglement sustainability improvement using optoelectronic converter in quantum radar (interferometric objectsensing)," IEEE Sensors Journal 21, 9054–9062 (2021).
- ⁶⁰L. Planat, Resonant and traveling-wave parametric amplification near the quantum limit, Ph.D. thesis, Université Grenoble Alpes [2020-....] (2020).
- ⁶¹C. Eichler and A. Wallraff, "Controlling the dynamic range of a josephson parametric amplifier," EPJ Quantum Technology 1, 2 (2014).
- ⁶²C. Macklin, K. O'brien, D. Hover, M. Schwartz, V. Bolkhovsky, X. Zhang, W. Oliver, and I. Siddiqi, "A near-quantum-limited josephson traveling-wave parametric amplifier," Science 350, 307–310 (2015).
- ⁶³L. Planat, R. Dassonneville, J. P. Martínez, F. Foroughi, O. Buisson, W. Hasch-Guichard, C. Naud, R. Vijay, K. Murch, and N. Roch, "Understanding the saturation power of josephson parametric amplifiers made from squid arrays," Physical review applied 11, 034014 (2019).
- ⁶⁴L. Chirolli, M. Carrega, and F. Giazotto, "The quartic blochnium: an anharmonic quasicharge superconducting qubit," Quantum 7, 1193 (2023).
- ⁶⁵M. Bell, I. Sadovskyy, L. Ioffe, A. Y. Kitaev, and M. Gershenson, "Quantum superinductor with tunable nonlinearity," Physical review letters 109, 137003 (2012).
- ⁶⁶F. Yan, Y. Sung, P. Krantz, A. Kamal, D. K. Kim, J. L. Yoder, T. P. Orlando, S. Gustavsson, and W. D. Oliver, "Engineering framework for optimizing superconducting qubit designs," arXiv preprint arXiv:2006.04130 (2020).
- ⁶⁷A. Salmanogli, H. Zandi, and M. Akbari, "Blochnium-based josephson junction parametric amplifiers: Superior tunability and linearity," IEEE Journal of Selected Topics in Quantum Electronics (2024).
- ⁶⁸S. Boutin, D. M. Toyli, A. V. Venkatramani, A. W. Eddins, I. Siddiqi, and A. Blais, "Effect of higher-order nonlinearities on amplification and squeezing in josephson parametric amplifiers," Physical Review Applied 8, 054030 (2017).
- ⁶⁹A. Salmanogli, H. S. Geçm, and E. Piskin, "Plasmonic system as a com-

- pound eye: image point-spread function enhancing by entanglement," IEEE sensors Journal **18**, 5723–5731 (2018).
- ⁷⁰M. Collett and C. Gardiner, "Squeezing of intracavity and traveling-wave light fields produced in parametric amplification," Physical Review A 30, 1386 (1984).
- ⁷¹A. Salmanogli, "Entangled state engineering in the 4-coupled qubits system," Physics Letters A 479, 128925 (2023).
- ⁷²E. Cha, N. Wadefalk, G. Moschetti, A. Pourkabirian, J. Stenarson, and J. Grahn, "Inp hemts for sub-mw cryogenic low-noise amplifiers," IEEE Electron Device Letters 41, 1005–1008 (2020).
- ⁷³A. Serafini, Quantum continuous variables: a primer of theoretical methods (CRC press, 2023).
- ⁷⁴C. Weedbrook, S. Pirandola, R. García-Patrón, N. J. Cerf, T. C. Ralph, J. H. Shapiro, and S. Lloyd, "Gaussian quantum information," Reviews of Modern Physics 84, 621–669 (2012).
- ⁷⁵G. Adesso and F. Illuminati, "Entanglement in continuous-variable systems: recent advances and current perspectives," Journal of Physics A: Mathematical and Theoretical 40, 7821 (2007).
- ⁷⁶B. Yurke, L. Corruccini, P. Kaminsky, L. Rupp, A. Smith, A. Silver, R. Simon, and E. Whittaker, "Observation of parametric amplification and deamplification in a josephson parametric amplifier," Physical Review A 39, 2519 (1989).
- ⁷⁷N. Bergeal, F. Schackert, M. Metcalfe, R. Vijay, V. Manucharyan, L. Frunzio, D. Prober, R. Schoelkopf, S. Girvin, and M. Devoret, "Phase-preserving amplification near the quantum limit with a josephson ring modulator," Nature 465, 64–68 (2010).
- ⁷⁸J. Y. Qiu, A. Grimsmo, K. Peng, B. Kannan, B. Lienhard, Y. Sung, P. Krantz, V. Bolkhovsky, G. Calusine, D. Kim, *et al.*, "Broadband squeezed microwaves and amplification with a josephson travelling-wave parametric amplifier," Nature Physics 19, 706–713 (2023).
- ⁷⁹D. G. Ahmad Salmanogli, "Optoelectronic based quantum radar," arXiv preprint arXiv:2007.10670 (2020).
- 80 R. G. Torromé, N. B. Bekhti-Winkel, and P. Knott, "Introduction to quantum radar," arXiv preprint arXiv:2006.14238 (2020).
- 81T. Gonzalez-Raya and M. Sanz, "Coplanar antenna design for microwave entangled signals propagating in open air," Quantum 6, 783 (2022).
- ⁸²M. Sanz, K. Fedorov, F. Deppe, and E. Solano, "Challenges in openair microwave quantum communication and sensing, arxiv e-prints," arXiv preprint arXiv:1809.02979 (2018).
- ⁸³S. R. Behera and U. Sinha, "Estimating the link budget of satellite-based quantum key distribution (qkd) for uplink transmission through the atmosphere," EPJ Quantum Technology 11, 66 (2024).
- ⁸⁴S. Jeon, J. Kim, D. Y. Kim, Z. Kim, T. Jeong, and S.-Y. Lee, "Single-mode phase-conjugate receiver for microwave quantum illumination with a lossy optical memory," Advanced Quantum Technologies , 2400627 (2025).
- 85 J. Wang, K. Petrovnin, P. J. Hakonen, and G. S. Paraoanu, "Observing the poisson distribution of a coherent microwave field with a parametric photon detector," IEEE Transactions on Quantum Engineering (2025).
- ⁸⁶P. Kurpiers, T. Walter, P. Magnard, Y. Salathe, and A. Wallraff, "Characterizing the attenuation of coaxial and rectangular microwave-frequency waveguides at cryogenic temperatures," EPJ quantum technology 4, 1–15 (2017)
- ⁸⁷D. Luong, S. Rajan, and B. Balaji, "Quantum two-mode squeezing radar and noise radar: Correlation coefficients for target detection," IEEE Sensors Journal 20, 5221–5228 (2020).
- ⁸⁸D. Luong, *Quantum Radar Signal Processing*, Ph.D. thesis, Carleton University (2023).
- ⁸⁹M. P. Da Silva, D. Bozyigit, A. Wallraff, and A. Blais, "Schemes for the observation of photon correlation functions in circuit qed with linear detectors," Physical Review A—Atomic, Molecular, and Optical Physics 82, 043804 (2010).
- ⁹⁰C. Eichler, D. Bozyigit, C. Lang, M. Baur, L. Steffen, J. M. Fink, S. Filipp, and A. Wallraff, "Observation of two-mode squeezing in the microwave frequency domain," Physical Review Letters 107, 113601 (2011).
- ⁹¹S. Barzanjeh, E. Redchenko, M. Peruzzo, M. Wulf, D. Lewis, G. Arnold, and J. M. Fink, "Stationary entangled radiation from micromechanical motion," Nature **570**, 480–483 (2019).
- ⁹²E. Cha, N. Wadefalk, G. Moschetti, A. Pourkabirian, J. Stenarson, and J. Grahn, "A 300-µw cryogenic hemt lna for quantum computing," in 2020 IEEE/MTT-S International Microwave Symposium (IMS) (IEEE, 2020) pp.

1299-1302.